Inactivation gating of potassium channels

Dissertation

zur Erlangung des Doktorgrades
-Dr.rer.nat.-
am Department Biologie der Universität Hamburg

Vorlegt von

Phanindra Velisetty

Hyderabad, India

Hamburg
August 2010

Genehmigt vom Fachbereich Biologie
der Fakultät für Mathematik, Informatik und Naturwissenschaften
an der Universität Hamburg
auf Antrag von Professor Dr. O. PONGS
Weitere Gutachterin der Dissertation:
Priv.-Doz. Dr. S. LÜTHJE
Tag der Disputation: 17. September 2010

Hamburg, den 03. September 2010

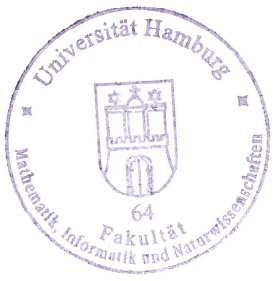

Professor Dr. Axel Temming
Leiter des Fachbereichs Biologie

UNIVERSITY OF CALIFORNIA, SAN FRANCISCO

BERKELEY • DAVIS • IRVINE • LOS ANGELES • RIVERSIDE • SAN DIEGO • SAN FRANCISCO SANTA BARBARA • SANTA CRUZ

Collin Spencer
UCSF Department of Neurology
513 Parnassus Avenue, Room S-268
San Francisco, CA 94143
Phone: (415) 476-2013
FAX: (415) 502-8512
E-Mail: cspencer@ucsf.neuroimmunol.org

July 29, 2010

Doctoral thesis for Phanindra Velisetty, University of Hamburg

To whom it may concern:

I, Collin Spencer, the undersigned, certify that I am a native English speaker. I have read Phanindra Velisetty's doctoral thesis draft and have provided the relevant advice in relation to English grammar and composition that should be incorporated into the final thesis. I affirm the thesis general language, grammar and spelling and should be readily understood by any native English speaker.

Sincerely,

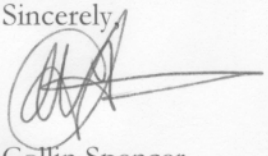

Collin Spencer

Contents

1. Introduction

1.1 Ion channels

Ion channels are macromolecular pores in cell membranes that establish and control the voltage gradient across cell membrane by allowing flow of ions down their electrochemical gradient. Ion channels are named depending on the type of ions they transport – sodium channels, potassium channels, chloride channels and calcium channels. Potassium channels (K^+ channels) are tetrameric membrane proteins consisting of four identical subunits that conduct K^+ ions across biological membranes and play a critical role in repolarization of action potential (Hille, 2001).

There are two main groups of potassium channels that are extensively studied as shown in figure 1.1 - potassium channels with two transmembrane segments (2 TM) M1 and M2 and six transmembrane segments (6TM) S1-S6. The 6TM K^+ channels exhibit additional transmembrane segments (S1-S4) that act as a voltage sensor domain.

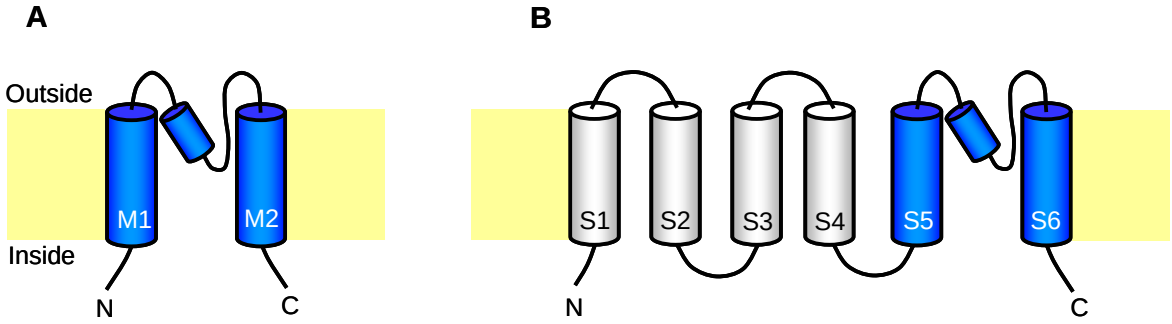

Figure 1.1: Cartoon representation of different transmembrane topologies of potassium channel subunits.
A. Potassium channels with two transmembrane domains M1 and M2 connected by a pore loop with a pore helix in it. (KcsA, MthK and Kir). **B**. Potassium channels with six transmembrane domains S1-S4 forming the voltage sensor domain and S5 and S6 forming the pore domain (Kv, KCNQ etc).

Potassium channels open and close in response to different stimuli. In voltage dependent potassium channels, changing the membrane potential leads to movement of voltage sensor and eventually opens the pore, a mechanism also called as electromechanical coupling (Long et al., 2005). Ligand gated potassium channels open upon binding of a ligand to the intracellular part of the channel (Yellen, 2002). In proton gated potassium channels binding of protons leads to channel opening. Thus, a change of intracellular pH from neutral to acidic or increase in intracellular H^+ concentration leads to opening of the channel. The most extensively studied proton gated potassium channel is the bacterial K^+ channel KcsA.

1.2 Structure of KcsA potassium channel

KcsA is a 160 amino acid protein, a homotetramer with four fold symmetry. The four identical subunits together form a central pore domain. Crystal structure data was obtained on C-terminally truncated KcsA (Cuello et al., 2010, Doyle et al., 1998). The domain consists of pore helix, turret region and selectivity filter (Zhou et al., 2001) as seen in figure 1.2 A. The pore is 45 Å long and divided into outer selectivity filter and inner water filled cavity, the latter being 10 Å wide. The N and C terminal regions of the protein face towards the intracellular surface of the membrane whereas the turret and selectivity filter face to the extracellular surface. The pore domain appears like an inverted tepee where the C-terminal regions of the protein cross over at the intracellular side due to the presence of a hinge. The selectivity filter consists of the consensus amino acid sequence TVGYG that is conserved in most K^+ channels (Doyle et al., 1998). The selectivity filter displays four potassium binding sites named 1-4 from outside to inside as shown in Figure 1.2 B.

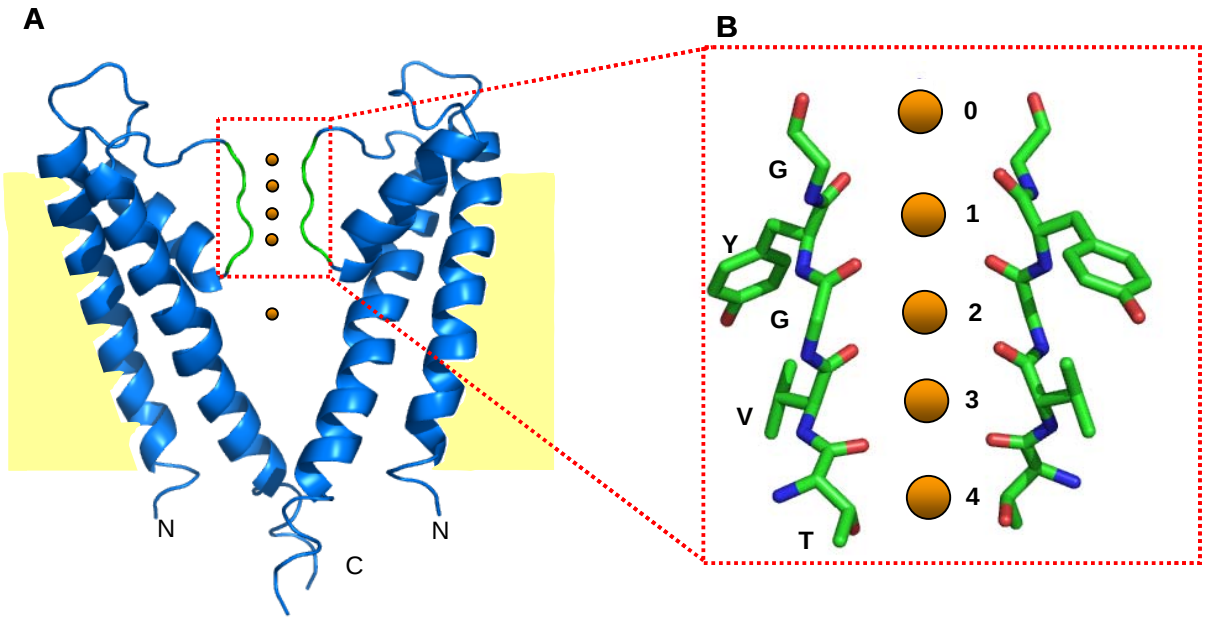

Figure 1.2: Cartoon representation of KcsA together with enlarged view of selectivity filter.
A. Ribbon representation of a potassium channel with only two subunits shown. The subunits in the front and the back are removed for clarity. Four potassium binding sites (orange spheres) are shown in the selectivity filter (green) and one in the vestibule. Cell membrane in indicated in yellow. **B.** Enlarged view of the selectivity filter in stick representation with potassium ion occupying 1/3 and 2/4 configurations. Blue: Nitrogen, green: carbon and red : oxygen atoms.

Binding sites 1-3 are formed by eight carbonyl oxygen atoms of the protein, two originating from each subunit. The binding site 4 is formed by four carbonyl oxygen atoms and four threonine side chain oxygen atoms. The potassium ions bind in a dehydrated state in two

configurations 1, 3 and 2, 4 with alternating water molecules (Morais-Cabral et al., 2001). There is an additional potassium binding site 0 at the extracellular side of the selectivity filter before binding site 1.

1.3 Activation and inactivation

In response to a stimulus, conformational changes in the inner helix bundle crossing leads to the opening of the inner gate, a process termed as activation (Kurata and Fedida, 2005). The inner gate is also called as activation gate or lower gate. The activation gate appears closed under resting conditions in all K^+ channels with an exception to Mthk where the activation gate stays wide open (Jiang et al., 2002b). Prolonged activation or frequent activity of K^+ channels leads to loss of conductivity, a process termed inactivation (Connor and Stevens 1971). Inactivation changes the signaling properties such as firing rate and duration of action potential. Two different kinds of K^+ channel inactivation can be distinguished: N-type and C-type inactivation. N-type inactivation also called ball and chain model that occurs when the N-terminal domain of the protein enters the pore and blocks from inside as shown in figure 1.3 A (Hoshi et al., 1990). N-type inactivation is rapid (ms range) and occurs when hydrophobic residues of the N terminal domain interact with the hydrophobic regions of the channel (Aldrich, 2001, Armstrong, 1969). It can be observed in *Shaker* from fruit fly as well as in several mammalian Kv channels (Rasmusson et al., 1995). N-type inactivation can be abolished by enzymatic digestion of the N-terminus (Murrell-Lagnado and Aldrich, 1993b) and sensitive to TEA^+ when applied intracellularly (Choi et al., 1991).

C-type inactivation is slow (s range) and occurs due to conformational changes in the selectivity filter after opening of the lower gate and eliminating ion conduction as shown in figure 1.3 B (Grissner and Cahalan, 1989, Yellen et al., 1994). Due to the fact that the selectivity filter collapses and aborts ion conduction it is also called upper gate or inactivation gate. Increasing the extracellular K^+ or using Rb^+ as permeant ion, which has a longer residence time in the selectivity filter slows down C-type inactivation (Kurata et al., 2005, (Shahidullah & Covarrubias, 2003). C-type inactivation is faster in the presence of N-type inactivation (Baukrowitz and Yellen, 1995). In KcsA coupling between the activation and inactivation gates was observed and hence channel opening leads to C-type inactivation due to cross talk between the gates. During C-type inactivation, selectivity filter backbone rearrangement first lead to loss of potassium ion at binding site 2 and subsequently at binding site 3 eventually leading to loss of ion conduction (Cuello et al., 2010a, Cuello et al., 2010b).

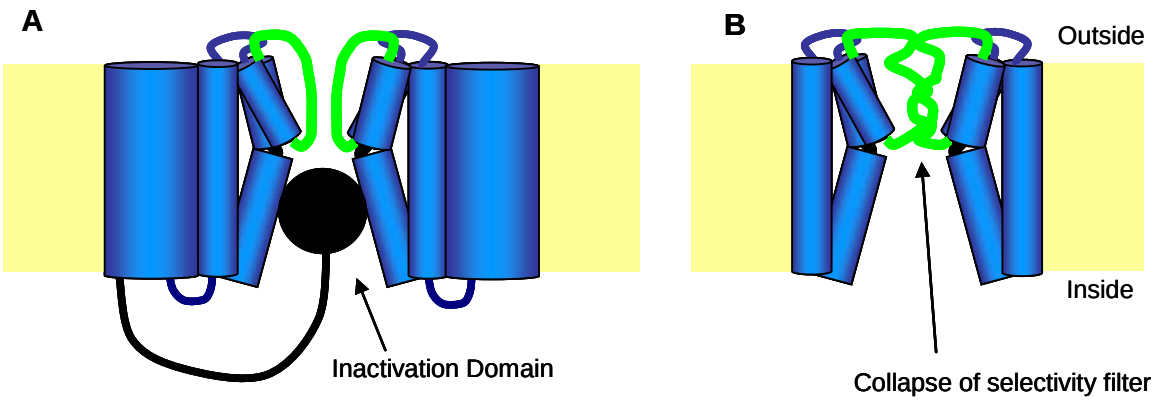

Figure 1.3: Cartoon representation of inactivation.
A. Cartoon representation of N-type inactivation. The inactivation domain is shown as a ball (black). **B**. Cartoon representation of C-type inactivation. The selectivity filter (green) is shown collapsed. In both A and B the transmembrane segments are shown as blue cylinders with the selectivity filter in green. Yellow regions indicate the membrane.

1.4 KcsA-Kv1.3 chimera

KcsA may be regarded as a structural archetype of the pore of Kv channels. A KcsA-Kv1.3 chimera was constructed due to several reasons - developing therapeutic agents, understanding potassium channel pharmacology, studying the biomolecular interaction of KcsA and animal toxins to the outer mouth of the pore. 13 amino acids corresponding to the scorpion toxin binding site in the turret region of Kv1.3 were transferred to KcsA. A sequence alignment of KcsA WT, KcsA-Kv1.3 and Kv1.3 is shown in figure 1.4. The chimera KcsA-Kv1.3 binds kaliotoxin with high affinity (Legros et al., 2000; Legros et al., 2002). Kaliotoxin binding to the KcsA-Kv1.3 in solid state NMR studies shows conformational rearrangements in the selectivity filter and also in the toxin residues conferring structural flexibility (Lange et al., 2006).

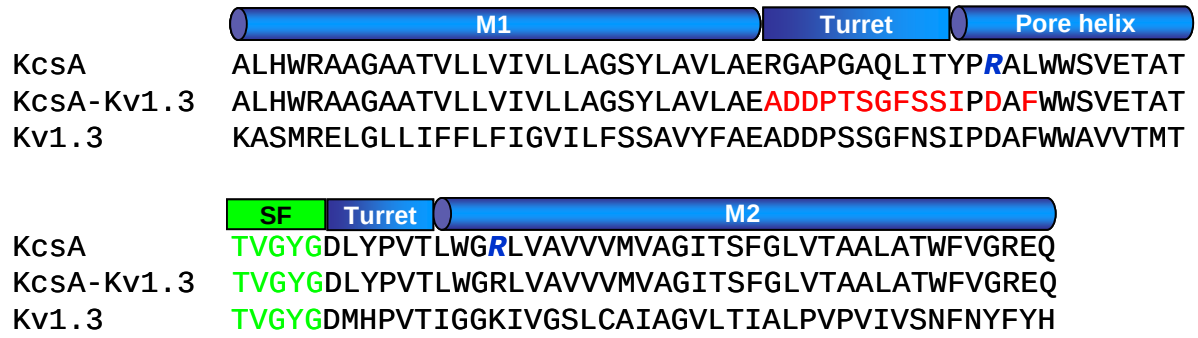

Figure 1.4: Sequence alignment of KcsA WT, KcsA-Kv1.3 and rKv1.3.
The selectivity filter residues are shown in green. Kv1.3 residues transferred onto KcsA are indicated in red in KcsA-Kv1.3 sequence. The amino acids indicated in blue italics are lipid binding residues that play a role in KcsA inactivation gating.

1.5 Gating of KcsA

In vitro KcsA opens at intracellular acidic pH in symmetrical K^+ solutions and remains closed at internal neutral or basic pH (Cuello et al., 1998, Heginbotham et al., 1999). If the K^+ concentration inside relative to outside is greater, KcsA opens even at neutral pH indicating that acidic intracellular pH is not the sole mechanism for activation (Zakharian and Reusch, 2004). Structural and functional studies were performed to locate the putative pH sensor. Mutation of C-terminal E118 and 120 together with N terminal H25 influence pH dependent gating (Cuello et al., 2010). The triple mutant E118A/E120A/H25R opens KcsA even at neutral pH. These residues together serve as pH sensor. The mechanism underlying pH dependent activation is proposed to rely on inter and intra subunit salt bridges and H-bonding between E118, E120 and H25, which stabilize the closed state at neutral pH. In acidic pH protonation of the glutamates leads to breakage of inter and intra subunit H-bonds and subsequently to opening of the activation gate (Thompson et al., 2008).

Functional studies of KcsA are difficult due to its low open probability (P_o ~ 0.2). Relatively low open probability of KcsA is due to the fact that the channel inactivates. Upon activation by protons, the channel opens and conducts ions, but subsequently inactivates by closing the upper gate (1-3 s). The steady state current remaining after inactivation is 10-30% of the peak amplitude (Chakrapani et al., 2007a, Cordero morales et al., 2006b). Single channel analysis showed that KcsA is characterized by a short open time interspaced with long closure times (Chakrapani et al., 2007b, Cordero morales et al., 2006b). Inactivation of the KcsA channel is thought to be similar to C-type inactivation of the *Shaker* Kv channel, i.e., due to conformational changes in the selectivity filter (Liu et al., 1996, Panyi et al., 1995, Cordero

morales et al., 2006b, Cuello et al., 2010a). Where as activation kinetics of KcsA are dependent on pH but not on voltage (Chakrapani et al., 2007a), inactivation kinetics is modulated by voltage but not by pH. Inactivation is faster and more complete at hyperpolarized potentials compared to depolarized potentials. Inactivation occurs even within the closed channel that is in the absence of ion conduction. Recovery from inactivation is also modulated by voltage and faster at hyperpolarized voltages (Chakrapani et al., 2007a). Alanine scanning mutagenesis shows aspartate at position 71 has a dramatic influence on inactivation in KcsA. A carboxl-carboxylate interaction between E71 and D80 inactivates the channel. Breaking this interaction by mutating E71 to A71 removes inactivation and increases the open probability to nearly 1 (P_o~1) with long open times and short closed times. Another point mutation R64A also has an influence on inactivation. R64 is believed to bind to the lipid molecules in the bilayer. Presumably disturbing the lipid protein packing by mutating this amino acid slows down inactivation. Neutralizing E71 makes KcsA voltage independent (Cordero morales et al., 2006a). KcsA inactivation follows activation and hence both activation and inactivation are coupled (Gao et al., 2005, Cuello et al., 2010b). A simple gating scheme may describe KcsA channel gating. It consists of closed, opened, opened inactivated and closed inactivated states. All the four states are in equilibrium and only the open state allows conduction of ions and all the other states do not conduct ions.

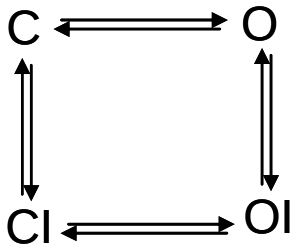

Activation due to opening of the activation gate leads to the transition from closed (C) to opened state (O). After activation loss of potassium ions at binding site 2 and 3 in the selectivity filter leads to closure of the inactivation gate and loss of ion conduction. The state is referred as OI (open inactivated). The activation gate closes following closure of the inactivation gate, a state referred as CI (closed inactivated). Recovery from inactivation occurs when the inactivation gate opens.

1.6 Interaction of lipid with KcsA

Ion channels interact with lipid through their transmembrane regions for structural stability and protein function (Deol et al., 2006, Williamson et al., 2002). Hydrophobic transmembrane regions of the channel are referred to as non annular sites where as lipid exposed regions of the channel are called annular sites or boundary regions. KcsA refolding and tetramer formation occurs in both zwitterionic and anionic phospholipids. Conduction of ions takes place only in the presence of anionic phospholipids (Henginbotham et al., 1998, Valiyaveetil et al., 2002). However the lipid head group structure whether it is PG, PA, PE or Cardiolipin is not important for KcsA function (Deol et al., 2006). Increasing the poly oleoyl phosphatidyl glycerol (POPG) content in the bilayer increases open probability (2.5% to 62%) indicating low open probability of KcsA arises due to lower anionic lipid i.e., percentage of PG in the lipid membrane for reconstitution of protein (Marius et al., 2008). The lipid molecule is bound at the interface between two subunits of the protein. The lipid binds to R64 of one protein subunit and R89 from the adjacent subunit of the protein. As the negatively charged lipid binds between two positively charged amino acids the repulsion between positively charged arginines is neutralized by the negatively charged lipid and hence the requirement of anionic lipid is essential for KcsA function (Marius et al., 2008, Valiyaveetil et al., 2002).

1.7 Objective

The objective of this study was to investigate the inactivation gating of K^+ channels. To this end KcsA-Kv1.3, KcsA WT and KcsA R64D were purified and reconstituted into lipid to form proteoliposomes. Inside out patch clamp technique was performed on proteoliposomes to study the inactivation gating. The focuses of the study were as follows:

- To study the influence of permeant ions like K^+ and Rb^+ on sequential gating activity of KcsA-Kv1.3. How is the inactivation gating of KcsA-Kv1.3 influenced by different extracellular and intracellular K^+?
- To investigate the influence of different lipidic environment on inactivation gating of KcsA WT and KcsA-Kv1.3.
- To identify the lipid binding amino acid and its influence on inactivation gating

2 Materials

2.1 Chemicals, enzymes and reagents

All the chemicals used in this study were of highest possible quality and purchased from Merck (Darmstadt, Germany), Roche (Berlin, Germany), Roth (Karlsruhe, Germany), Sigma & Aldrich (Munich, Germany) unless mentioned specifically. Enzymes, kits and Molecular weight standards were obtained from Clontech (Saint Germain-en-Laye, France), Invitrogen (Darmstadt Germany), MBI fermentas (St-Leon-Rot, Germany), Stratagene (Agilent technologies, Waldbronn, Germany) and Qiagen (Hilden, Germany) respectively.

2.2 Bacterial strain

XL 1-Blue	recA1, endA1, gyrA96, thi-1, hsdR17, supE44, relA1, lac [F'proAB, $lac^qZ\Delta M15$, Tn10 (tet^R)]^C, Stratagene
E.coli M15 [pREP4]	Nal^S, Str^S, Rif^S, Thi^-, Ara^+, Gal^+, Mtl^-, F^-, $RecA^+$, Uvr^+, Lon^+, Qiagen

2.3 Expression vectors and channel protein

pQE32	Expression vector for recombinant protein from *E.coli* with amino terminal RGS-Histidine tag (Qiagen, Hilden, Germany)
pQE70	Expression vector for recombinant protein from *E.coli* with carboxy terminal Histidine tag (Qiagen, Hilden, Germany)

2.4 Kits

GFX Micro Plasmid Prep Kit	Plasmid minipreps (Amersham Biosciences, München Germany)
Nucleobond AX system	Plasmid midipreps (Macherey & Nagel, Düren, Germany)

3 Methods

3.1 Molecular biology and protein purification

3.1.1 Preparation of competent bacteria

10 mL of LB medium was inoculated with a single colony from an LB plate and grown at 37 ºC overnight in shaking cvonditions. 100 mL of LB media was inoculated with 1 mL of overnight culture and incubated at 37 ºC until an $O.D._{600}$ of 0.5. The flasks were then removed from the shaker and placed on ice for 10 min. The culture was centrifuged (SIGMA 2 K 15) at 5000 RPM for 10 min at 4 ºC. The bacterial pellet was suspended gently in ice cold TB buffer and placed on ice for 10 min. The suspension was centrifuged at 5000 RPM for 10 min at 4 ºC. The pellet was resuspended in 20 mL TB buffer and 1.5 mL DMSO was added with gentle swirling. Aliquots of the suspension were prepared in precooled eppendorf tubes and frozen immediately in liquid nitrogen and stored at -80 ºC.

3.1.2 Transformation

30 ng of PQE32 DNA and PQE70 DNA were transformed separately into 100 µL of *E.coli* M15 competent cells and incubated for 20 min on ice followed by 42 ºC water bath for 90 s and immediately placed on ice for 2-3 min. 500 µL of SOC medium was added to the preparation and incubated at 37 ºC for 1 hour under shaking conditions. The grown culture was then centrifuged (Centrifuge 5430, eppendorf) at 3000 RPM for 1 min and the pellet was dissolved in 50 µL of SOC medium and plated on LB agar plates containing ampicillin and kanamycin. The plates were incubated overnight at 37 ºC.

3.1.3 Expression culture

A day culture was prepared by picking up a single colony from the LB agar plates and inoculated into 10 mL of SB medium containing ampicillin and kanamycin. 1mL from the day culture was used to inoculate 50 mL (1:50 ratio) of overnight culture containing ampicillin, kanamycin and 0.1% glucose. The expression culture was then inoculated with overnight culture. The culture was incubated at 37 ºC until an $O.D._{600}$ of ~ 0.37 and shifted to lower

temperature at 26 ºC until an $O.D._{600}$ of ~ 0.8. 0.5 mM IPTG was added and the culture was grown for 6-7 h. The culture was then centrifuged (Sorvall RC 5C) at 10,500 g for 15 min and the pellet was stored at -80 ºC.

3.1.4 Cell lysis and purification

The pellet was dissolved in BAK buffer pH 7.0 + tablet complete without EDTA and lysed using French press (3 cycles at 20,000 psi). The cell lysate was centrifuged at 15000 RPM for 45 min and the supernatant was centrifuged at 104,000 g for 1 h in an ultracentrifuge. The pellet was dissolved in BBK buffer pH 7.0 + 40 mM DM and incubated overnight at 4 ºC in slow stirring conditions. The suspension was then centrifuged (Sorvall Discovery 90) at 70,000 g for 1 h in an ultracentrifuge. Imidazole was added to the supernatant to a final concentration of 30 mM and pH was adjusted to 7.8. The supernatant was then mixed with Ni-NTA agarose which is already washed with the washing buffer to be used and incubated at 4 ºC for 90 min on a rocking platform. The column was washed with 10 column volumes of BBK buffer pH 7.8, 4 mM DM and 30 mM imidazole. The protein was then eluted into different tubes using 7 column volumes of BBK buffer pH 7.8, 4 mM DM and 400 mM imidazole.

3.1.5 SDS gel Electrophoresis

8 µL of the eluted protein sample was mixed with 16 µL of Laemmli buffer and incubated at 95 ºC for 5 min. The samples were loaded into wells of PAGE gel. 10 µL of Novex protein standard was mixed with 10 µL of the loading dye and loaded onto the first well. Electrophoresis was performed at 200 mV in MES Buffer until the flow front reached the bottom. The gel was stained using simply blue safe stain (Invitrogen) for 1 h and destained in water for 1 h.

3.1.6 Measurement of protein concentration

The concentration of the purified protein was measured using wave scan. 100 µL of control buffer (BBK buffer pH 7.8, 4 mM DM and 400 mM imidazole) was used as reference. 1:10 dilution of the protein with the control buffer was made and absorbance at 280 nm was

observed. According to the amino acid number and MW the value for absorbance was calculated and for KcsA-Kv1.3, one abosorbance is equal to 0.57 mg/mL.

3.1.7 Preparation of lipid and desalting of the protein

The lipid was dissolved in chloroform and methanol in a 2:1 (v/v) ratio and dried at room temperature under nitrogen atmosphere. The lipid was then lyophilized overnight to remove residual chloroform and methanol. The lyophilized sample was dissolved in BBK buffer, pH 7.4 containing detergent, vortexed and kept in ultrasonic water bath for 15 min. Desalting of the protein was done using PD-10 columns (GE Health care). The column was equilibrated with 6-7 column volumes of 50 mM Na-P pH 7.4, 50 mM NaCl and 4 mM DM. Sample was added to the column and eluted into different tubes with 50 mM Na-P pH 7.4, 50 mM NaCl and 4 mM DM. The sample is mixed with lipid vesicles before it gets turbid.

3.1.8 Preparation of proteoliposomes

Protein and lipid were mixed in a 1:100 (mass: mass) and left for 2 h at room temperature on a shaker. After integration of protein into the lipid membrane calbiosorb beads were added to an Econo pac column (14 cm, Bio Rad laboratories) and equilibrated with 50 mM Na-P pH 7.4, 50 mM NaCl without DM. The proteoliposome sample was added to the column and left for 2 h at room temperature on a shaker. The sample was eluted with 50 mM Na-P pH 7.4, 50 mM NaCl without DM and centrifuged at 179,000 g at 4 ºC. The proteoliposome pellet was dissolved in 200 mM NaCl and 10 mM MOPS and again centrifuged for 1 h at 4 ºC. The pellet was incubated at 4 ºC overnight in 200 mM NaCl and 10 mM MOPS and dissolved the next day.

3.1.9 Preparation of poly-l-lysine slides

30 mM cover slips were sorted out in porcelain racks and placed into acetone for 20 min on a rocking platform. Acetone was discarded and the slides were washed with distilled water five times and rinsed with 100% ethanol for 10 min. The slides were again washed with distilled water five times. The porcelain rack containing the slides was baked at 180 ºC for 2 h and wrapped with aluminium foil and incubated for one more hour. The aluminium foil was

removed under the laminar flow hood. The cover slips were coated with 3 mL of poly-l-lysine hydrobromide (30,000-70,000 MW) by overnight incubation at 4ºC. The slides were washed five times with distilled water and stored in refrigerator until use.

3.1.10 Drying and rehydration of proteoliposomes

The slides were dried and placed on a small petri dish. 20 µL of rehydration buffer was added to the edges of the dried proteoliposome and rehydrated for 2-3 h. The bath solution was added to the dish prior to electrophysiological measurements.

3.1.11 Solutions for molecular biology and protein purification

Solutions for bacterial expression

LB medium	10	g/L	NaCl
	10	g/L	peptone
	5	g/L	yeast extract

Ampicillin was added to a final concentration of 100µg/mL and kanamycin to 25µg/mL.

LB agar	1	L	LB medium
	15	g/L	agar
SB medium	5	g/L	NaCl
	25	g/L	peptone
	15	g/L	yeast extract
IPTG	1	mM	IPTG in H_20
SOB	0.5	g/L	NaCl
	1	mL/L	KCl
	20	g/L	peptone
	5	g/L	yeast extract
SOB	1	L	SOB
	!	M	glucose

Solutions for protein expression			
diethylpyrocarbonate (DEPC)-H_20	0.01	% (v-v)	DEPC in H_20
TB buffer	3	g/L	PiPES
	2.2	g/L	$CaCl_2$
	18.6	g/L	KCl
	10.9	g/L	$MnCl_2$
BAK buffer	50	mM	MOPS
	150	mM	KCl
BBK buffer	200	mM	$NaH_2PO_4.H_20$
	200	mM	$Na_2HPO_4.7H_20$
	150	mM	KCl
Na-P, NaCl buffer	50	mM	$NaH_2PO_4.H_20$
	50	mM	$Na_2HPO_4.7H_20$
	50	mM	NaCl
Solutions for proteoliposomes			
Borate buffer	100	mM	Boric acid (pH 8.5)
0.01 % PLL	1	L	Borate buffer
	0.1	g/L	PLL
Rehydration buffer (KCl)	150	mM	KCl
(pH 7.0)	0.1	mM	EDTA
	0.01	mM	$CaCl_2$
	5	mM	HEPES
Rehydration buffer (NaCl)	150	mM	NaCl
(pH 7.0)	0.1	mM	EDTA
	0.01	mM	$CaCl_2$
	5	mM	HEPES

3.2 Electrophysiology

3.2.1 Experimental set up

A conventional patch clamp set up was used for electrophysiological recordings. The petri dish containing the proteoliposomes was filled with K^+ solution, pH 7.0. K^+ concentration was changed depending on different experiments. The petri dish was placed under inverted light microscope Axiovert 405M (Carl Zeiss MicroImaging GmbH, Hamburg, Germany). The patch pipette with a reference electrode is connected to the headstage that was mounted on a micromanipulator Patchman (Eppendorf AG, Hamburg, Germany). Patch pipettes were made of borosilicate glass (GB 150-10, Science products, Hofheim, Germany) and pulled using an automatic puller (DMZ - Universal Puller, Zeitz – Instruments Vertriebs GmbH, Martinsried, Germany). The pipettes were polished using a polisher (ID 03, Zeiss instruments). The pipettes were coated with sigmacote for better sealing of the pipette with the membrane. Different pH and K^+ solutions was added to inside out patch using gravity flow connected to a piezzo driven double barrel perfusion system and adjusted near to the patch. Automatic switch of solutions is obtained by connecting a SF-77B perfusion fast step (Warner Instrument Corporation) to the amplifier that allows the automatic fast switch of the solutions upon starting the experiment. The time duration of the switch for which the solution is changed is controlled in the pulse protocol. Suction system is connected to the chamber to remove the continuous perfusion of the solution. The bath chamber, microscope, micromanipulator and head stage were placed on air table with pressure cylinders to eliminate vibrations. The whole set up is placed in a faraday cage and connected to the ground to reduce electrical noise. Recordings and data acquisition were controlled by an EPC-9 patch clamp amplifier. Combined with pulse/pulsefit software (HEKA Elektronik, Dr Schulze GmbH, Lambrecht/Pfalz, Germany). The amplifier was connected to a computer. The patch clamp circuit is shown in figure 3.1.

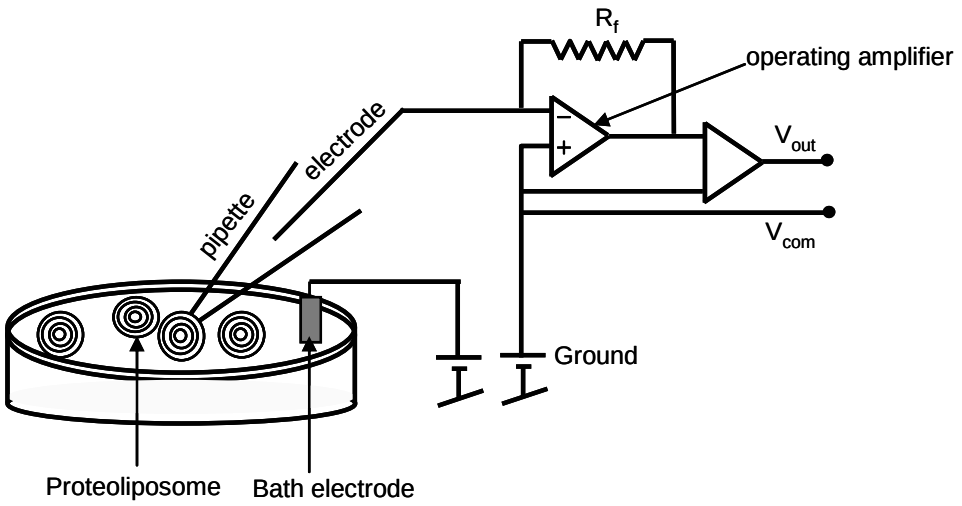

Figure 3.1: A circuit of the patch clamp.
The current measured flows back through the feedback resistor R_f. the pipette is connected to the operating amplifier. V_{out} indicates the measured current and V_{com} indicates the voltage command.

3.2.2 Electrical recording of KcsA-Kv1.3

Activity of KcsA-Kv1.3 channel reconstituted into asolectin lipid was measured using inside out patch clamp technique. Symmetrical 200 mM KCl was used for the initial experiments to check the inactivation properties of KcsA. Both the pipette solution (pH 7.0) and perfusion (pH 7.0 & 4.0) contained 200 mM KCl. Patches were held at 0 mV and after obtaining a gigaseal the pipette was withdrawn from the cell to form inside out configuration. The patches were depolarized to +100 mV. After depolarization the pH was changed manually from 7.0 to 4.0 for 4-5 seconds and switched back to pH 7.0 and then to 0 mV. The experimental set up for the recording is shown in figure 3.2 and the solutions for the above mentioned experimental protocol are detailed in Table 3.1.

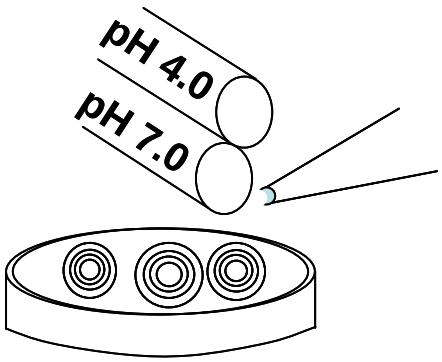

Figure 3.2: Electrical recordings of KcsA-Kv1.3.
Inside out patch clamp configuration for recording KcsA-Kv1.3 reconstituted in proteoliposomes. After getting a gigaseal the patches were exposed to piezzo driven double barrel containing pH 7.0 and 4.0

Table 3.1: Solutions for inside out patch clamp recording of KcsA-Kv1.3 reconstituted in asolectin proteoliposomes.

Solutions	
Bath and pipette (pH 7.0)	200 mM KCl, 10 mM MOPS
Perfusion (pH 7.0)	200 mM KCl, 10 mM MOPS
Perfusion (pH 4.0)	200 mM KCl, 10 mM MOPS

3.2.3 Inactivation and recovery from inactivation of KcsA-Kv1.3 in different extracellular and intracellular K^+ concentrations

The starting concentration for potassium dependent inactivation experiments was 150 mM KCl. KcsA-Kv1.3 in asolectin proteoliposomes was first measured in symmetrical 150 mM KCl solutions. Then the extracellular K^+ concentration (pipette solution) was lowered from 150 to 0 mM (8 mM, 1 mM, 200 μM, 1 μM and 0 K^+). Bath and the pipette solutions were always neutral (pH 7.0). The intracellular K^+ concentration (perfusion) was maintained at 150 mM (pH 7.0 and 4.0). Patches were held at 0 mV. Outward currents were measured by depolarizing to +100 mV and the change in pH from 7.0 to 4.0 was made by automatic switch (SF-77b fast perfusion step). Recovery from inactivation of KcsA-Kv1.3 in these different extracellular K^+ concentrations was measured using increasing interpulse interval duration. The solutions for outward currents are detailed in Table 3.2. Next pipette and bath solution were set at 150 mM K^+, pH 7.0 and were perfused with different intracellular concentrations ranging from 150 to 0 mM (1 mM, 200 μM, 10 μM, 1 μM and 0 K^+). The patches were held at -100 mV and the inward currents were measured by hyperpolarizing to -300 mV and change in pH was obtained by automatic switch. Recovery from inactivation was measured for inward currents by increasing interpulse interval duration. For both the outward and inward currents the ionic strength was kept constant by replacing K^+ with Na^+. Bath solution was set to 0 K^+, pH 7.0 for all the measurements. The solutions for inward currents are mentioned in Table 3.3.

Table 3.2: Solutions for measuring KcsA-Kv1.3 inactivating outward currents and recovery from inactivation.

Symmetrical 150 mM K^+	Pipette (pH 7.0)	150 mM KCl, 10 mM MOPS
	Perfusion (pH 7.0)	150 mM KCl, 10 mM MOPS
	Perfusion (pH 4.0)	150 mM KCl, 10 mM MOPS
Asymmetrical 8 mM K^+	Pipette (pH 7.0)	8 mM KCl, 142 mM NaCl, 10 mM MOPS
	Perfusion (pH 7.0)	150 mM KCl, 10 mM MOPS
	Perfusion (pH 4.0)	150 mM KCl, 10 mM MOPS
Asymmetrical 1 mM K^+	Pipette (pH 7.0)	1 mM KCl, 149 mM NaCl, 10 mM MOPS
	Perfusion (pH 7.0)	150 mM KCl, 10 mM MOPS
	Perfusion (pH 4.0)	150 mM KCl, 10 mM MOPS
Asymmetrical 200 μM K^+	Pipette (pH 7.0)	200 μM KCl, 149.800 mM NaCl, 10 mM MOPS
	Perfusion (pH 7.0)	150 mM KCl, 10 mM MOPS
	Perfusion (pH 4.0)	150 mM KCl, 10 mM MOPS
Asymmetrical 1 μM K^+	Pipette (pH 7.0)	1 μM KCl, 149.999 mM NaCl, 10 mM MOPS
	Perfusion (pH 7.0)	150 mM KCl, 10 mM MOPS
	Perfusion (pH 4.0)	150 mM KCl, 10 mM MOPS
Asymmetrical 0 mM K^+	Pipette (pH 7.0)	0 μM KCl, 150 mM NaCl, 10 mM MOPS
	Perfusion (pH 7.0)	150 mM KCl, 10 mM MOPS
	Perfusion (pH 4.0)	150 mM KCl, 10 mM MOPS

Table 3.3: Solutions for measuring KcsA-Kv1.3 inactivating inward currents and recovery from inactivation.

Symmetrical 150 mM K^+	Pipette (pH 7.0)	150 mM KCl, 10 mM MOPS
	Perfusion (pH 7.0)	150 mM KCl, 10 mM MOPS
	Perfusion (pH 4.0)	150 mM KCl, 10 mM MOPS
Asymmetrical 1 mM K^+	Pipette (pH 7.0)	150 mM KCl, 10 mM MOPS
	Perfusion (pH 7.0)	1 mM KCl, 149 mM NaCl, 10 mM MOPS
	Perfusion (pH 4.0)	1 mM KCl, 149 mM NaCl, 10 mM MOPS
Asymmetrical 200 µM K^+	Pipette (pH 7.0)	150 mM KCl, 10 mM MOPS
	Perfusion (pH 7.0)	200 µM KCl, 149.800 mM NaCl, 10 mM MOPS
	Perfusion (pH 4.0)	200 µM KCl, 149.800 mM NaCl, 10 mM MOPS
Asymmetrical 10 µM K^+	Pipette (pH 7.0)	150 mM KCl, 10 mM MOPS
	Perfusion (pH 7.0)	10 µM KCl, 149.990 mM NaCl, 10 mM MOPS
	Perfusion (pH 4.0)	10 µM KCl, 149.990 mM NaCl, 10 mM MOPS
Asymmetrical 1 µM K^+	Pipette (pH 7.0)	150 mM KCl, 10 mM MOPS
	Perfusion (pH 7.0)	1 µM KCl, 149.999 mM NaCl, 10 mM MOPS
	Perfusion (pH 4.0)	1 µM KCl, 149.999 mM NaCl, 10 mM MOPS
Asymmetrical 0 mM K^+	Pipette (pH 7.0)	150 mM KCl, 10 mM MOPS
	Perfusion (pH 7.0)	0 µM KCl, 150 mM NaCl, 10 mM MOPS
	Perfusion (pH 4.0)	0 µM KCl, 150 mM NaCl, 10 mM MOPS

3.2.4 Measurement of KcsA-Kv1.3 in Rb^+ solution

Both outward and inward currents of KcsA-Kv1.3 in asolectin lipid were measured in symmetrical 150mM Rubidium solutions. Recovery from inactivation is measured in inward and outward directions using interpulse interval duration. For outward currents the patches were held at 0 mV and depolarized to +100 mV followed by a switch in the pH. For inward currents the patches were held at -100 mV and hyperpolarized to -300 mV followed by a pH switch. The solutions used are listed in Table 3.4

Table 3.4: Solutions for measuring KcsA-Kv1.3 currents in symmetrical Rb^+ solutions.

Solutions	
Bath and pipette (pH 7.0)	150mM RbCl, 10mM MOPS
Perfusion (pH 7.0)	150mM RbCl, 10mM MOPS
Perfusion (pH 4.0)	150mM RbCl, 10mM MOPS

3.2.5 Inactivation of KcsA-Kv1.3 at different voltages in different K^+ concentrations

To see whether inactivation is influenced by driving force or voltage, inactivation at different voltages was measured. KcsA-Kv1.3 in asolectin lipid was measured at different voltages in different K^+ concentrations. The voltage drop at different concentrations was the same. The reversal potential was calculated for each concentration and the patches were held at that potential. In symmetrical 150 mM K^+ solutions the holding potential was 0 mV and the voltage was changed in either directions up to +/- 150 mV in 25 mV steps. For asymmetrical 20 mM K^+ solutions the patches were held at -50 mV and hyperpolarized to -250 mV in 25 mV steps and depolarized to +100 mV in 50 mV steps. For asymmetrical 1 μM solutions the patches were held at -100 mV and depolarized to +100 mV and hyperpolarized to -300 mV in 50 mV steps. The driving force was calculated and plotted against inactivation tau. The solutions were mentioned in Table 3.5.

Driving force = (Holding potential - Reversal potential) -Test potential.

Table 3.5: Solutions for measuring KcsA-Kv1.3 inactivation at different voltages.

Symmetrical 150 mM K^+	Pipette (pH 7.0)	150 mM KCl, 10 mM MOPS
	Perfusion (pH 7.0)	150 mM KCl, 10 mM MOPS
	Perfusion (pH 4.0)	150 mM KCl, 10 mM MOPS
Asymmetrical 20 mM K^+ outside	Pipette (pH 7.0)	20 mM KCl, 130 mM NaCl, 10 mM MOPS
	Perfusion (pH 7.0)	150 mM KCl, 10 mM MOPS
	Perfusion (pH 4.0)	150 mM KCl, 10 mM MOPS
Asymmetrical 1 μM K^+ outside	Pipette (pH 7.0)	1 μM KCl, 149.999 mM NaCl, 10mM MOPS
	Perfusion (pH 7.0)	150 mM KCl, 10 mM MOPS
	Perfusion (pH 4.0)	150 mM KCl, 10 mM MOPS
Asymmetrical 20 mM K^+ inside	Pipette (pH 7.0)	150 mM KCl, 10 mM MOPS
	Perfusion (pH 7.0)	20 mM KCl, 130 mM NaCl, 10 mM MOPS
	Perfusion (pH 4.0)	20 mM KCl, 130 mM NaCl, 10 mM MOPS
Asymmetrical 1 μM K^+ inside	Pipette (pH 7.0)	150 mM KCl, 10 mM MOPS
	Perfusion (pH 7.0)	1 μM KCl, 149.999 mM NaCl, 10 mM MOPS
	Perfusion (pH 4.0)	1 μM KCl, 149.999 mM NaCl, 10 mM MOPS

3.2.6 Measurement of KcsA WT and KcsA-Kv1.3 in different lipid composition.

Measurements in different lipid mixtures were performed in symmetrical 50 mM K^+ solutions for both KcsA WT and KcsA-Kv1.3. First both the proteins were reconstituted separately into asolectin lipid and inside out patch clamp technique was used. Patches were held at 0 mV and depolarized to +100 mV at pH 4.0. Both KcsA WT and KcsA-Kv1.3 were reconstituted into combination of different phospholipid mixtures: DOPC: DOPG (7:3), DOPC: DOPG (5:5), DOPC: DOPA (7:3), DOPC: Cardiolipin (7:3). Holding potential was 0 mV and depolarized to +100mV at pH 4.0. Structures of the lipids used in the experiments are shown in figure 3.3 and the solutions used are listed in Table 3.6.

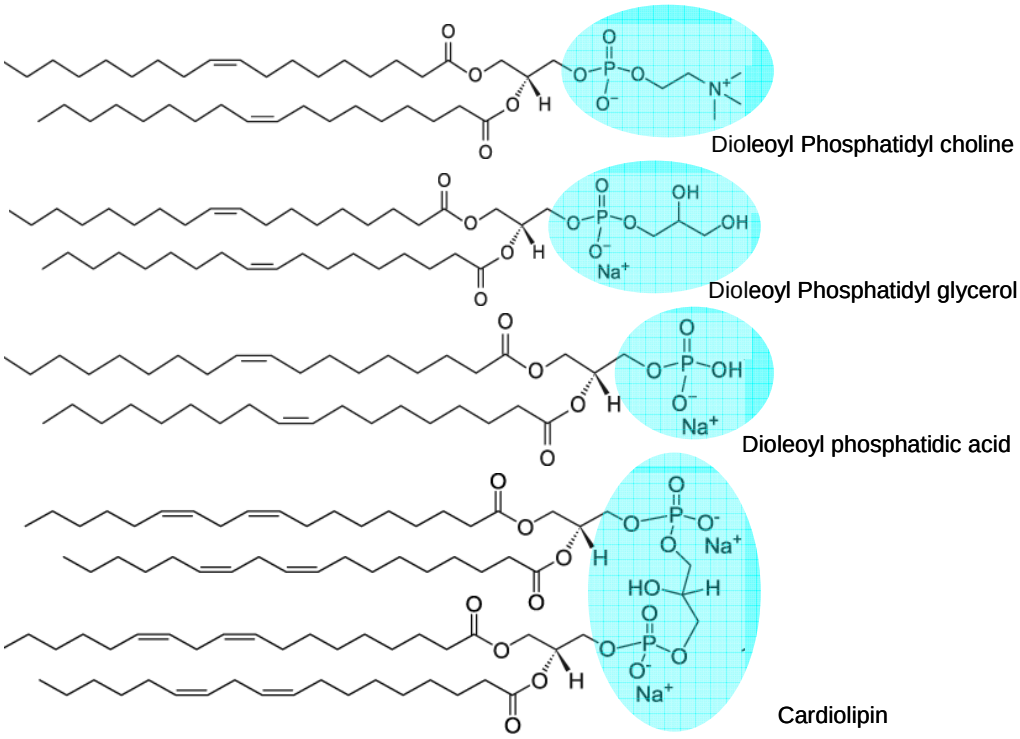

Figure 3.3: Chemical structure of different phospholipids.

The head groups of the lipid are colored.

Table 3.6: Solutions for measuring KcsA-WT and KcsA-Kv1.3 in different phospholipid mixtures.

Symmetrical 50 mM K^+	Pipette (pH 7.0)	50 mM KCl, 10 mM MOPS
	Perfusion (pH 7.0)	50 mM KCl, 10 mM MOPS
	Perfusion (pH 4.0)	50 mM KCl, 10 mM MOPS

3.2.7 Measurement of KcsA-R64D in symmetrical K+ solutions

A point mutant KcsA-R64D reconstituted into asolectin lipid was measured in symmetrical 50 mM K^+ solutions. The patches were held at 0 mV and depolarized to +100 mV and the data were compared with that of KcsA WT and KcsA-Kv1.3 in asolectin lipid. Solutions are mentioned in Table 3.7.

Table 3.7: Solutions for measuring KcsA-R64D in symmetrical K^+ solutions.

Symmetrical 50 mM K^+	Pipette (pH 7.0)	50 mM KCl, 10 mM MOPS
	Perfusion (pH 7.0)	50 mM KCl, 10 mM MOPS
	Perfusion (pH 4.0)	50 mM KCl, 10 mM MOPS

3.3 Data analysis

Data analysis and calculations were performed using Pulsefit (HEKA), Kaleidagraph(version 3.5, Synergy software, Reading, USA) and Mathcad 13.0 (PTC, Neeham, USA). Recordings were performed at a sampling rate of 1 KHz and the files were exported in ASC format using pulsefit. Current traces were analyzed and normalized to 1 using Kaleidagraph. Data points from a particular current trace at different time points were collected and analyzed using Mathcad 13.0. Kinetics of KcsA gating was analysed using below mentioned equation. The time constants for activation and inactivation together with peak and steady state current were analyzed for each and every experiment. Currents were well described by fitting to the data a Hodgkin—Huxley-related formalism ($I=I_0 m(t)^4\ h(t)$) with one activation (τ_{act}) and one inactivation time constant (τ_{inact}) (Roeper *et al*, 1997).

$$I1(t1) := A1 \cdot \left(1 - e^{\frac{-t1}{\tau 1}}\right)^4 \cdot \left[\frac{(A1 - Ao) \cdot e^{\frac{-t1}{\tau 2}} + Ao}{A1}\right]$$

A1 indicates the estimated peak current reached in the absence of inactivation. Ao indicates the steady state current remaining after inactivation. τ1 gives the time constant of activation and the exponent 4 in the first half of the equation assumes that movement of four subunits is required to open a channel. τ2 gives the time constant of inactivation.

The normalized I_{ss}/I_{max} in outward and inverse inactivation time constants in inward currents plotted against K^+ concentration were fitted with Hill equation with 1 and 4 binding sites to calculate the dissociation constants.

$$f(x)= a0+(a1-a0)/(1+(a2/x)) – 1 \text{ binding site}$$
$$f(x)= a0+(a1-a0)/(1+(a2/x)^4) – 4 \text{ binding sites}$$

a0 is the lower value of time constant and a1 is the higher value. a2 is the estimated midpoint. Exponent indicates the binding sites.

Recovery from inactivation is measured by taking the peak current amplitudes of each pulse during recovery and normalized to the peak current amplitude of the first pulse. The values

taken in this way are plotted and calculated the time constant for recovery from inactivation using a simple formula in mathcad.

$$I(t) := 1 - A \cdot e^{\frac{-t}{\tau}}$$

A indicates the peak current, t is the time scale during recovery and τ gives the time constant for recovery from inactivation.

4 Results

4.1 Protein expression and Gel analysis

The potassium channel KcsA-Kv1.3 was expressed in *E.coli* containing the PQE32 vector and purified as described in methods (3.1.3 and 3.1.4). Samples of different purification steps were loaded onto SDS polyacrylamide gel to analyze size and purity of the recombinant protein. Bands can be seen in the lane from the pellet of ultracentrifugation in which the crude protein was present. The flow through from Ni NTA column contains all other contaminating protein bands. No protein in the tetramer size (60 KD) was seen. One protein band was observed in lanes 5, 6, 7 and 8 corresponding to KcsA-Kv1.3 indicated in figure 4.1. The protein was pure enough for further electrophysiological experiments.

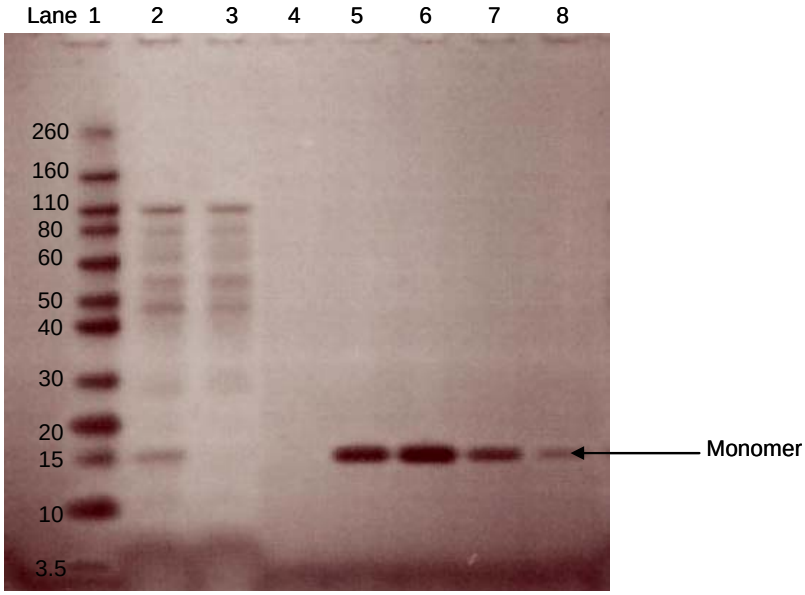

Figure 4.1: Gel image showing different purification steps of KcsA-Kv1.3 protein.
Lane 1 - Novex sharp protein standard in KD, lane 2 - pellet from ultracentrifugation, lane 3 - flow through from Ni-NTA, lane 4 -wash, lane 5,6,7,8 –elution fractions 1,2,3,4 (for further details see methods).

4.2 Electrophysiological recordings on KcsA-Kv1.3 containing proteoliposomes

Inside out patch clamp experiments on proteoliposomes containing KcsA-Kv1.3 chimera reconstituted into asolectin lipid were performed. Depolarization from -100 mV to +100 mV and change of the internal pH from 7.0 to 4.0 in symmetrical 200 mM K^+ solutions opened the

channel for a short time and upon prolonged activation the channel showed inactivation (figure 4.2) with a time constant τ_{inact}=0.58±0.06 s (n=4 and s.e.m). The channel closed upon bringing back the internal pH to 7.0. Amplitude of the steady state current remaining after a 4 s test pulse was 24±1% (n=4 and s.e.m) of the peak amplitude. Activation and inactivation properties of KcsA-Kv1.3 chimera were similar those one published for KcsA WT (Cordero morales 2006b).

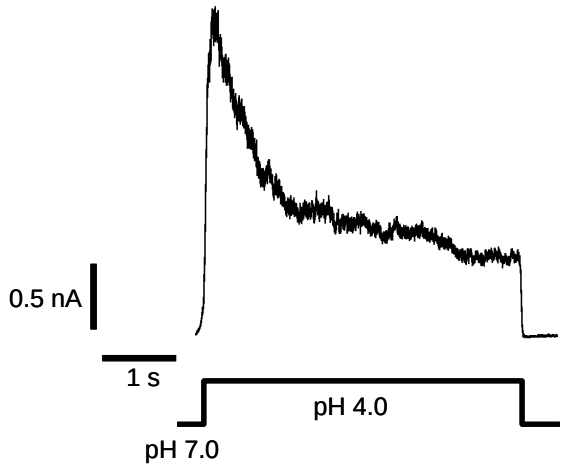

Figure 4.2: Representative current trace of KcsA-Kv1.3 in proteoliposomes.
Activation by switching acidic pH together with depolarization to +100 mV for the time indicated. $[K^+]_{out}$– 200 mM and $[K^+]_{in}$ – 200 mM. Time scale was indicated as a bar.

4.2.1 Effect of extracellular K^+ concentration, ($[K^+]_{out}$) on KcsA-Kv1.3 inactivation recovery from inactivation

Next, gating properties of KcsA-Kv1.3 was studied in different $[K^+]_{out}$. It was reported previously (Zhou et al, 2001) that in low extracellular K^+, the KcsA selectivity filter collapses, whereas high extracellular K^+ stabilizes it. KcsA-Kv1.3 was measured in different $[K^+]_{out}$ and $[K^+]_{in}$ to investigate the influence of K^+ on KcsA-Kv1.3 inactivation. In controls, KcsA-Kv1.3 outward currents were measured by depolarizing test pulses to +100 mV at pH 4.0 in symmetrical 150 mM K^+. The channel inactivated with a time constant of τ_{inact}=0.37±0.04 s (n=5 and s.e.m) in symmetrical K^+ solutions and the amplitude of steady state current remaining after inactivation was 26±2% (n=5 and s.e.m) of the peak current amplitude. The extracellular K^+ concentration was reduced from 150 to 8 mM, 1 mM, 1 µM and respectively 0 K^+ while keeping intracellular K^+ constant. The ionic strength in asymmetrical solutions was kept constant by replacing with Na^+. KcsA-Kv1.3 inactivation was accelerated with a P value of 0.0002 (student T-test) and the steady state current amplitude remaining after inactivation decreased (figure 4.3A). Steady state current amplitude was for 1 mM - 15±5%

(n=4 and s.e.m), 1 µM (n=3 and s.e.m) and 0 K^+ it is 10±1% (n=3 and s.e.m) of the peak current amplitude. The activation was not affected but $[K^+]_{out}$ significantly influenced KcsA-Kv1.3 τ_{inact} (figure 4.3 B). A plot of steady state current amplitude divided by maximum current amplitude I_{ss}/I_{max} versus $[K^+]_{out}$ revealed that I_{ss}/I_{max} titrates with $[K^+]_{out}$ (figure 4.3 C), showing a K_D of 0.9 mM with a maximal I_{ss}/I_{max} value of 0.44 at 150 mM $[K^+]_{out}$ and a minimum I_{ss}/I_{max} value of 0.02 at 0 $[K^+]_{out}$. The inactivation time constant and the steady state current (I_{ss}/I_{max}) was sensitive to $[K^+]_{out}$ or the electrochemical K^+ gradient.

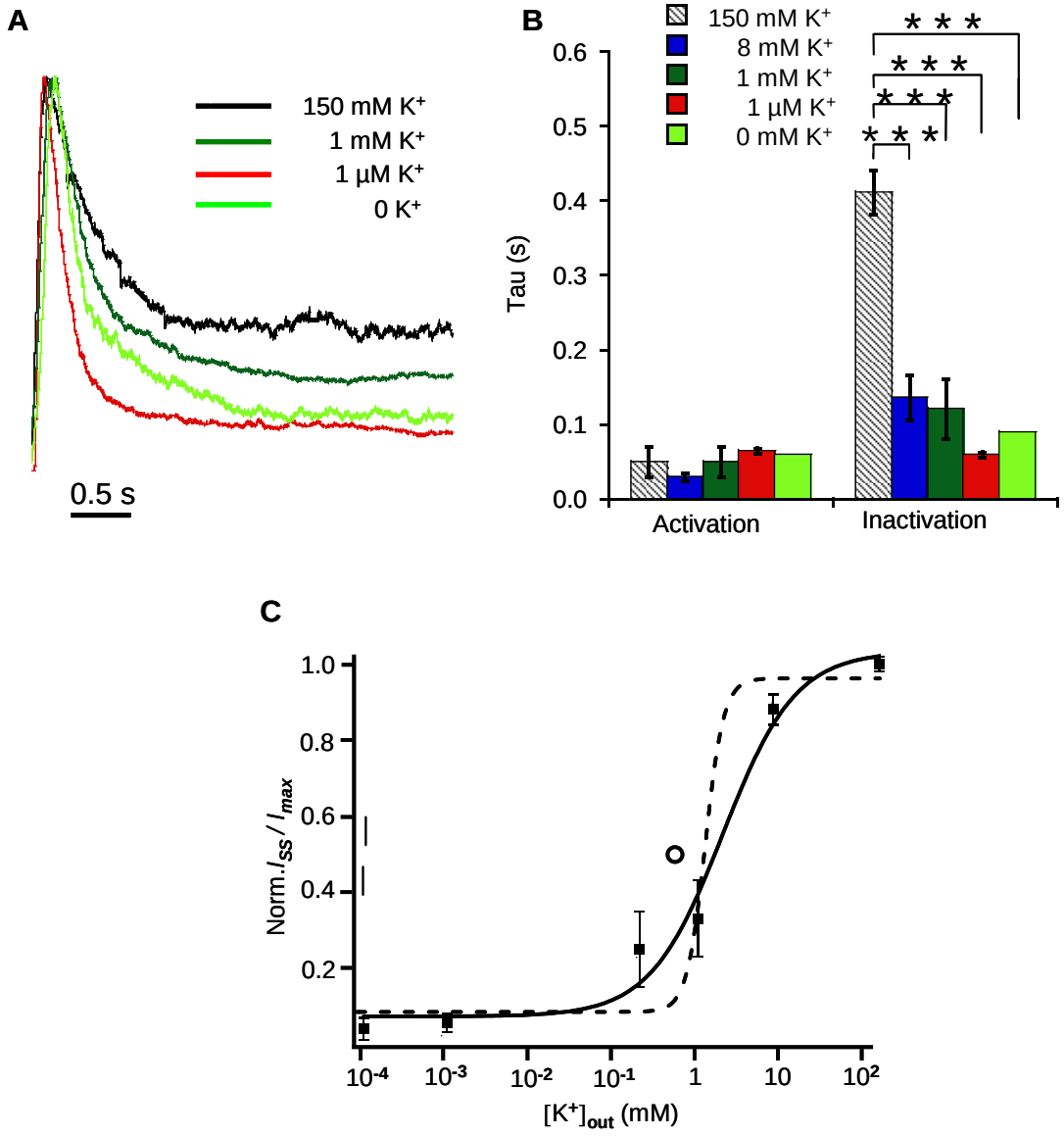

Figure 4.3: Influence of different $[K^+]_{out}$ on KcsA-Kv1.3 outward currents.
A. Current traces of KcsA-Kv1.3 in asolectin lipid. The traces are scaled to 1. Bar indicates time. Different K+ concentrations are colour coded as indicated. **B.** Time constants for activation and inactivation are indicated in bar diagram. The error bars are s.e.m. P value is 0.0002 when symmetrical 150 mM was compared to all other $[K^+]_{out}$ concentrations **C.** Normalized steady-state current amplitudes I_{ss}/I_{max} plotted against $[K^+]_{out}$. Solid line represents fitted curve to the dose-response data with one binding site and dotted line represents with four binding sites (o) with K_D for external K^+ binding of 0.9 mM. Error bars are s.e.m. (n=5–14). (o)—K_D for extracellular K^+-binding site on KcsA (Lockless et al, 2007).

Recovery of the KcsA-Kv1.3 channel from inactivation was measured in different $[K^+]_{out}$ using a double pulse protocol (figure 4.4 A, bottom) with increasing interpulse intervals between the test pulses. Peak current amplitudes during recovery were normalized to the peak amplitude of the first trace plotted against interpulse time. The data were well described with a single exponential fit (figure 4.4 B). The channel recovered completely in different $[K^+]_{out}$ so that peak current amplitude after recovery was similar to the peak current amplitude of the first pulse. No significant difference was observed for the time constants for recovery from inactivation in different $[K^+]_{out}$ (figure 4.4 C). The time constant was τ_{rec}=2±0.5 s (n=3, and s.e.m).

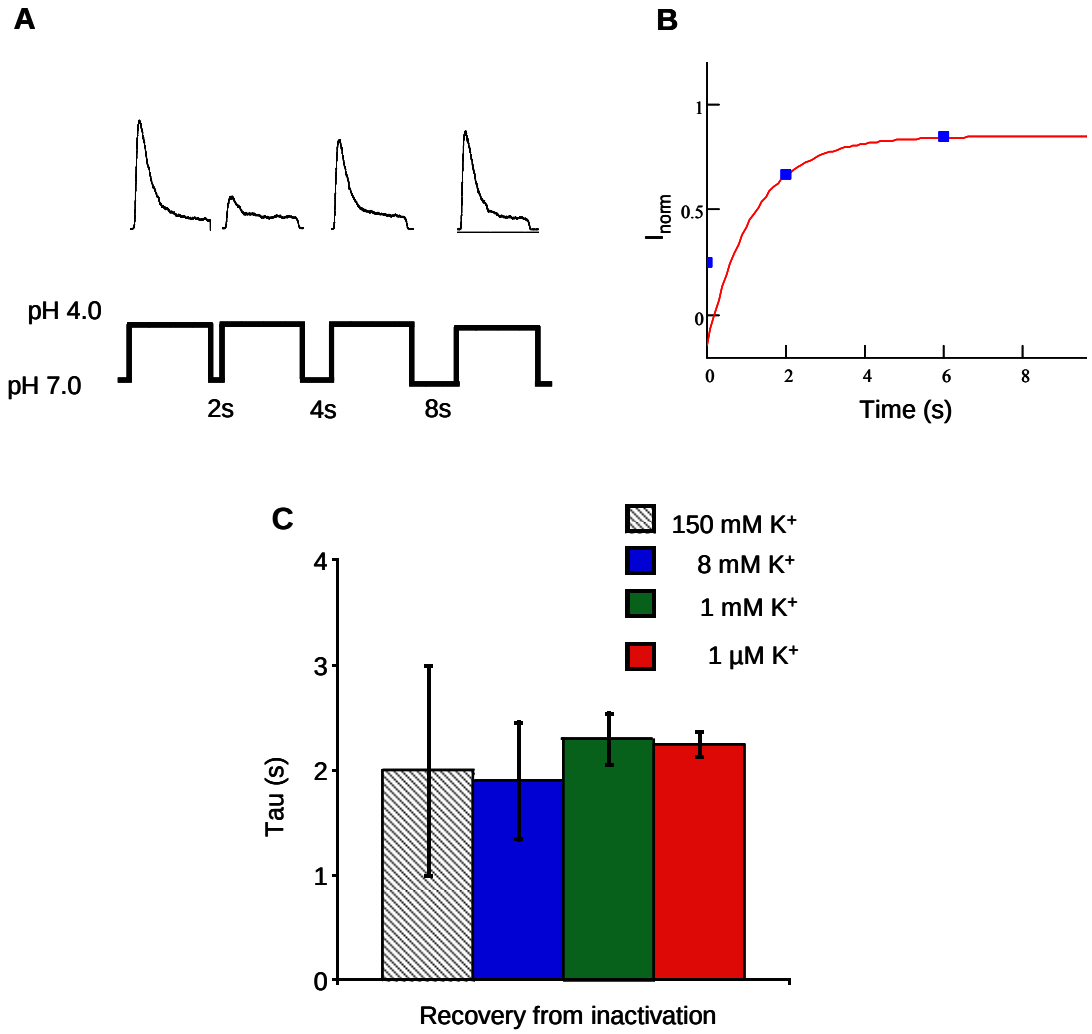

Figure 4.4: Effect of different $[K^+]_{out}$ on KcsA-Kv1.3 recovery from inactivation in outward currents.

A. (Above) Current traces recorded in asymmetric 1 mM $[K^+]_{out}$. The peak current amplitude of the final trace is similar to that of the starting trace. (Below) Pulse protocol used for recovery from inactivation. The interpulse interval duration increases exponentially 2, 4, 8 and 16s. **B.** Single exponential fit to calculate the recovery from inactivation time constants. **C.** Bar diagram showing the time constants calculated for recovery from inactivation at different $[K^+]_{out}$ (n=3 for each). Error bars are s.e.m.

4.2.2 Effect of intracellular K^+, ($[K^+]_{in}$) on KcsA-Kv1.3 inactivation and recovery from inactivation

Next, the influence of $[K^+]_{in}$ on KcsA–Kv1.3 gating properties was investigated. Inward currents were elicited in symmetrical 150 mM K^+ solutions by hyperpolarizing test pulses to -300 mV. Rapid and complete inactivation was observed with a time constant τ_{inact}=0.14±0.02 s (n=7, s.e.m). No change in inactivation kinetics was observed (figure 4.5 A) upon reducing the $[K^+]_{in}$ from 150 mM to 1 mM, 200 µM, 10 µM, 1 µM, and 0 K^+ respectively, keeping $[K^+]_{out}$ constant. The most important observation, was that $[K^+]_{in}$ significantly accelerated KcsA–Kv1.3 inactivation. A plot of the inactivation rate $1/\tau_{inact}$ versus $[K^+]_{in}$ showed that τ_{inact} titrates with $[K^+]_{in}$ (figure 4.5 B), revealing an internal K^+-binding site (one) with K_D=6.5 µM.

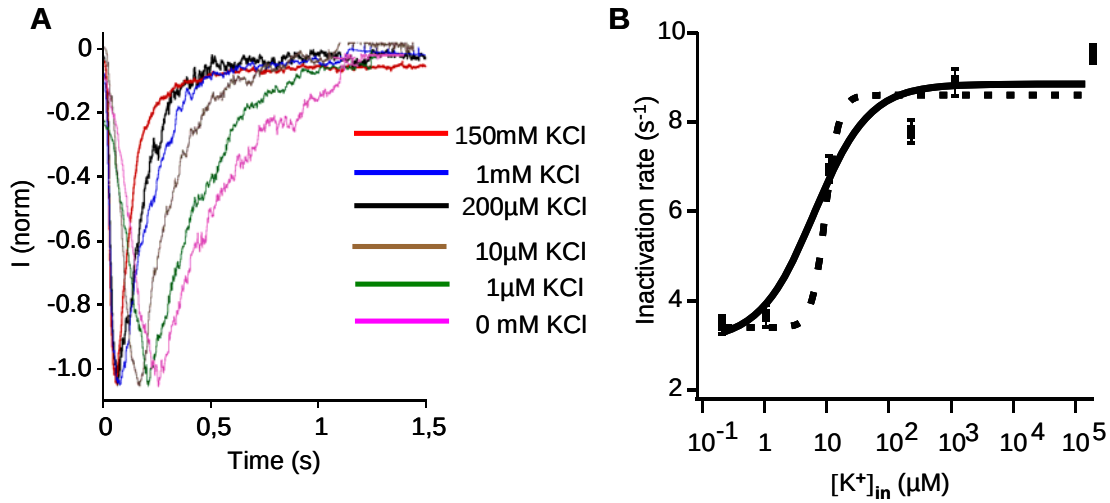

Figure 4.5: Influence of different $[K^+]_{in}$ on KcsA-Kv1.3 inward currents.
A. Normalized KcsA–Kv1.3 inward currents (I_{norm}) recorded at -100 mV with different internal K^+ ($[K^+]_{in}$) solutions. Outside (pipette) solution contained 150 mM KCl. (**B**) $[K^+]_{in}$ sensitivity of inactivation rate. Error bars are s.e.m. (n=5–12). K_D value of 6.5 µM was obtained by fitting a smooth curve to the dose-response data. Solid line represents the fit with one binding site whereas the dotted line was with four binding sites.

In contrast, the time course of KcsA–Kv1.3 recovery from inactivation was K^+ insensitive Recovery from inactivation was measured with a similar protocol as used for outward currents. The only difference was that hyperpolarizing test pulses to different negative potentials (figure 4.6 A). Peak amplitudes during recovery were normalized to the peak amplitude of the initial trace and fitted with single exponential function (figure 4.6 B). The time course for recovery from inactivation was K^+ insensitive =1.9±0.2 s (n=3, s.e.m). No significant differences were observed for τ_{rec} in different $[K^+]_{in}$ (figure 4.6B)

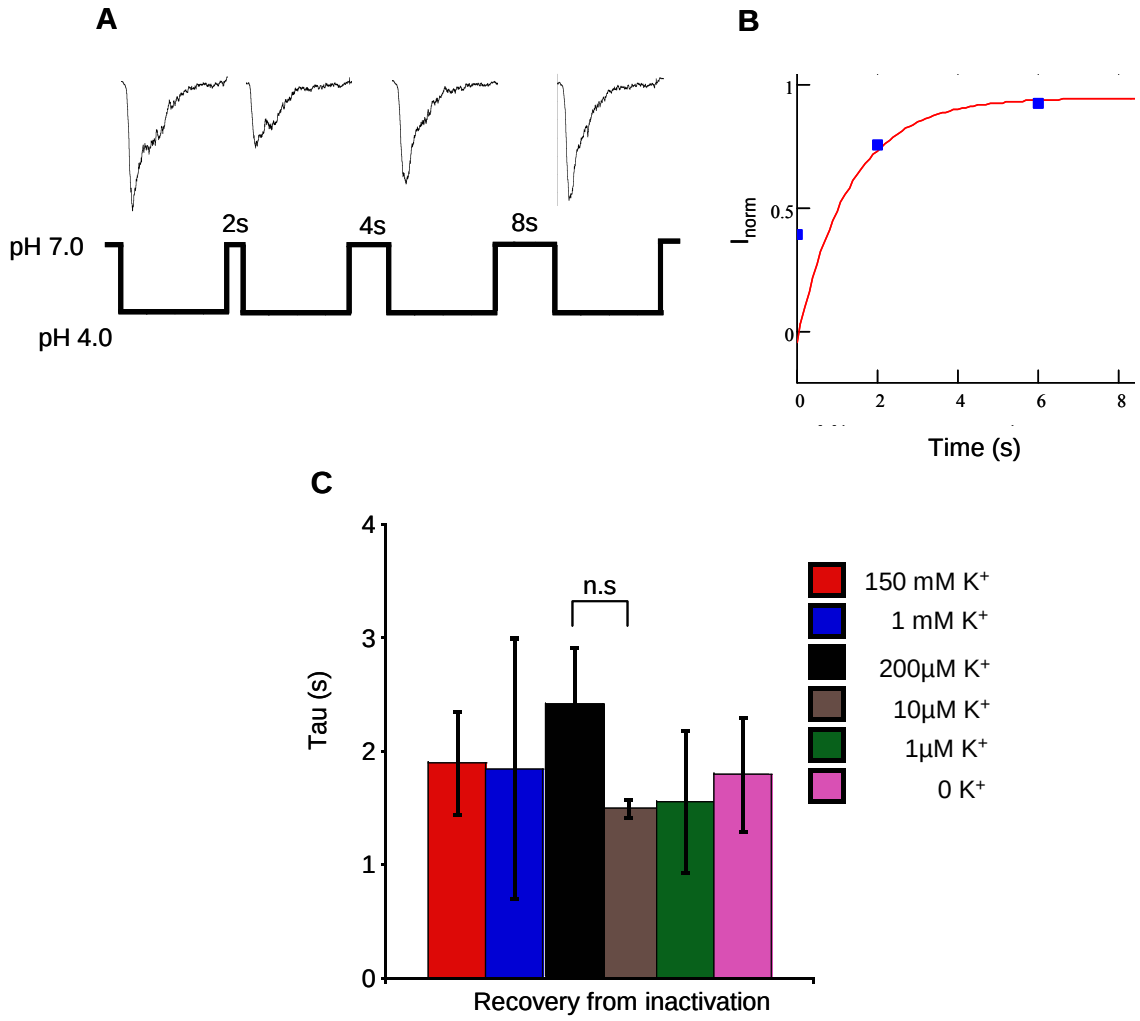

Figure 4.6 Effect of different $[K^+]_{in}$ on KcsA-Kv1.3 recovery from inactivation in inward currents. **A**. (Above) Representative current traces recorded in asymmetric 1mM $[K^+]_{in}$. The peak current amplitude of the final trace is similar to that of the starting trace. (Below) Pulse protocol used for recovery from inactivation. The interpulse interval duration increases exponentially 2, 4 and 8 s. **B.** Single exponential fit to calculate the recovery from inactivation time constants. **C.** Bar diagram showing the time constants calculated for recovery from inactivation at different $[K^+]_{in}$ (n=3 for each). Error bars are s.e.m.

4.2.3 Effect of Rb^+ on KcsA-Kv1.3 activation and inactivation

Rb^+ ions, which also permeate potassium channels slow C type inactivation of Kv channels (Lopez Barneo et al., 1993; Shahidullah and Covarrubias, 2003). The influence of Rb^+ on KcsA-Kv1.3 inactivation was investigated in symmetrical 150 mM Rb^+ solutions. KcsA-Kv1.3 activation was unaffected by Rb^+. The time constant τ_{act}=0.07±0.02 s (n=3, s.e.m) was similar to that of K^+ mediated outward currents with time constant τ_{act}=0.05±0.02 s (figure 4.7A, left). A significant difference in inactivation kinetics however, was observed with τ_{inact} for Rb^+=2.63±0.14 s compared to τ_{inact} for K^+=0.33±0.04 s (figure 4.7 A middle). Time constants for recovery from inactivation (τ_{rec}) in symmetrical Rb^+ (τ=2.3±0.4 s) (n=3 and

s.e.m) and K^+ mediated outward currents (τ=2±0.5 s) (n=7 and s.e.m) were essentially identical (figure 4.7 A right).

Activation and inactivation kinetics of inward currents were slowed 2-3 fold by Rb^+ in comparision to K^+ .The difference was statistically insignificant (P=0.07, student T test; n=3, s.e.m) (figure 4.7 B, left and middle). Time constants for recovery from inactivation in symmetrical Rb^+ (τ_{rec}=1.9±0.5 s, n=3, s.e.m) and K^+ mediated outward currents (τ_{rec}=2±0.5 s, n=6, s.e.m) were essentially identical (figure 4.7 B right) and similar to outward currents. An important observation was that inactivation of Rb^+ mediated KcsA-Kv1.3 outward currents (τ_{inact} =2.63±0.14 s) was relatively slow compared to inactivation of Rb^+ mediated inward currents (τ_{inact} =0.26±0.04 s) (figure 4.7A and B, middle). Rb^+ slowed down the inactivation kinetics of outward currents, but not of inward currents whereas the recovery from inactivation is unaffected in both outward and inward currents.

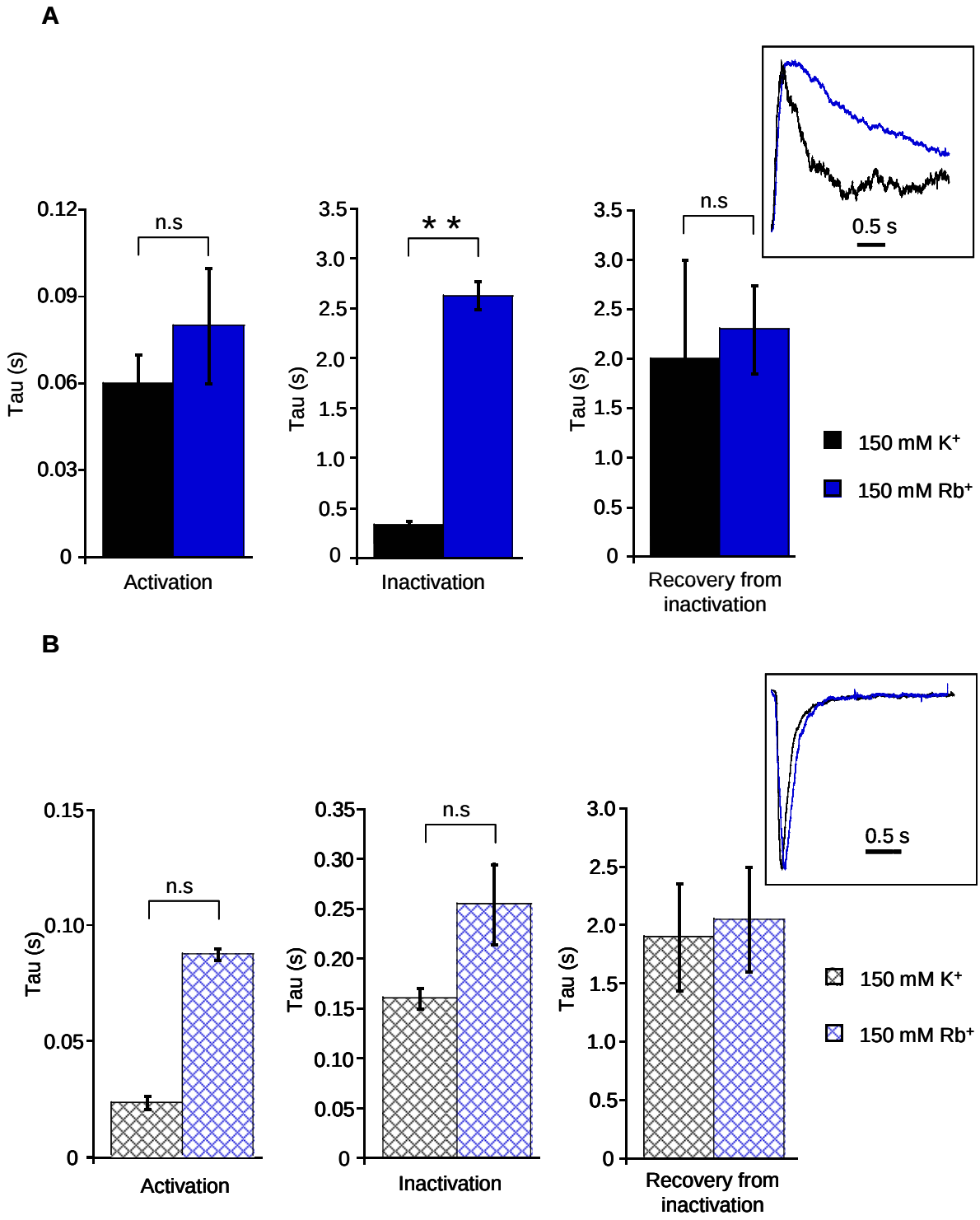

Figure 4.7: Influence of symmetrical Rb^+ and K^+ on KcsA-Kv1.3 outward and inward currents. **A**. Comparision of activation (left), inactivation (middle) and recovery from inactivation (right) time constants (n=5 for K^+ and 7 for Rb^+, error bars are s.e.m) between K^+ and Rb^+ mediated outward currents. P value is 0.002 for inactivation. n.s indicates no significant difference. **Inset:** comparision of representative current traces that were scaled to 1 and bar indicates time. **B.** Comparision of activation (left), inactivation (middle) and recovery from inactivation (right) time constants (n=5 for K^+ and 7 for Rb^+, error bars are s.e.m) between K^+ and Rb^+ mediated inward currents. **Inset:** comparision of representative current traces that were scaled to 1 and bar indicates time

4.2.4 Effect of different voltages on KcsA-Kv1.3 inactivation in different K^+ solutions

Next, the influence of driving force on the observed K^+ dependent inactivation was investigated. Thus, KcsA-Kv1.3 currents were measured at different voltages in different K^+ solutions. In symmetrical 150 mM K^+ solutions, strong depolarizing or strong hyperpolarizing test pulse (+150 mV or -150 mV) from a holding potential of 0 mV accelerated KcsA-Kv1.3 inactivation. Less depolarizing or hyperpolarizing test pulses (+50 mV or -50 mV) resulted in slowing of inactivation. The mean values of τ_{inact} were similar for a particular voltage drop in either direction and form a bell shaped curve (figure 4.7 A left). In symmetrical 150mM K^+ solutions τ_{inact} plotted against driving force resulted in a bell shaped curve similar to τ_{inact} plotted against voltage (figure 4.7 A right). In asymmetrical 20 mM $[K^+]_{out}$ (20 mM outside and 150 mM inside) and asymmetrical 20 mM $[K^+]_{in}$, (20 mM inside and 150 mM outside) stronger depolarization and hyperpolarization (-250 or +100 mV) fastened inactivation when compared to less voltage drop like in symmetrical K^+ solutions. The data points form a bell shaped curve (figure 4.7 B left). A plot of driving force vs τ_{inact} resulted in a bell shaped curve and small voltage dependence is observed (figure 4.7 B right). Similar kind of results was observed for asymmetrical 1 µM $[K^+]_{out}$ (1 µM outside and 150 mM inside) and 1 µM $[K^+]_{in}$ (1 µM inside and 150 mM outside) (figure 4.7 C left and right). Comparision of inactivation time constants difference ($\Delta\tau_{inact}$) at a difference of 50 mV driving force (Δ driving force) versus K^+ concentration (figure 4.8D) showed that the time constants were different. The inactivation observed can be attributed to differences in K^+.

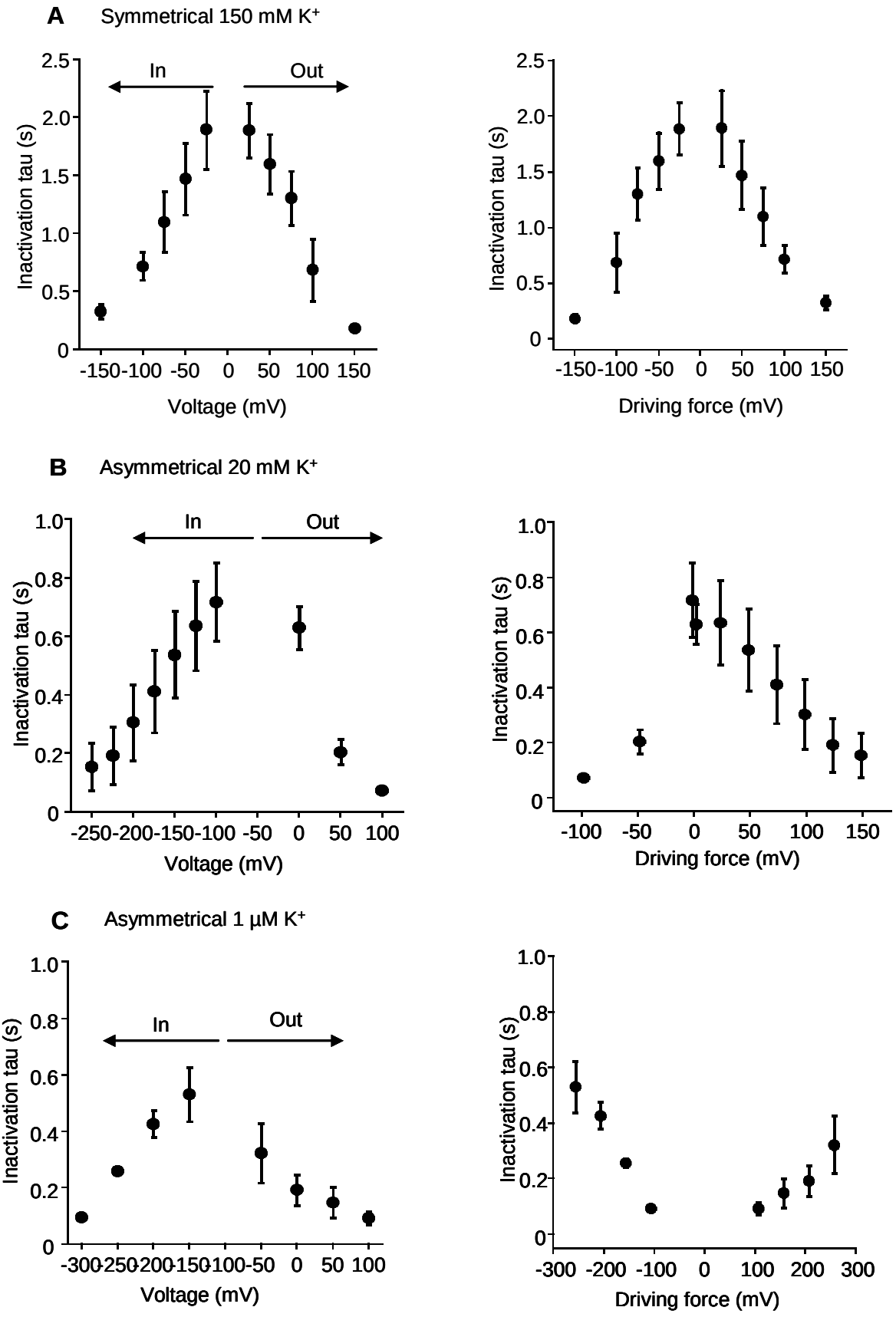
A
Symmetrical 150 mM K+
In
Out
Inactivation tau (s)
Voltage (mV)
Driving force (mV)
B
Asymmetrical 20 mM K+
C
Asymmetrical 1 µM K+

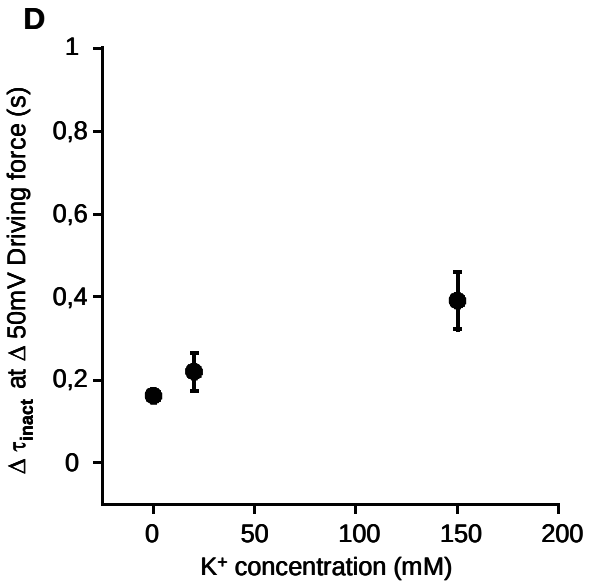

Figure 4.8: Influence of driving force and voltage on KcsA-Kv1.3 outward and inward currents. **A**. **Left:** Inactivation time constants plotted against voltage in symmetrical 150 mM K^+ solutions. Inactivation time constants were 0.1 - 0.3 s at +150 and -150 mV. Holding potential was 0 mV. **Right:** τ_{inact} plotted against driving force in symmetrical 150 mM K^+ formed bell shaped curve**. B. Left:** In asymmetrical 20 mm K^+ solutions, the holding potential was -50 mV. For outward currents 20mM $[K^+]_{out}$, 150 mM $[K^+]_{in}$ was used and for inward currents 20 mM $[K^+]_{in}$ and 150 mM $[K^+]_{out}$ was used. **Right:** τ_{inact} plotted against driving force in asymmetrical 20 mM $[K^+]_{out}$ and 20 mM $[K^+]_{in}$. **C. Left:** In asymmetrical 1 µM K^+ solutions holding potential of -100mV was used. For outward currents 1 µM $[K^+]_{out}$ and 150 mm $[K^+]_{in}$ and vice versa for inward currents were used. **Right:** τ_{inact} plotted against driving force in asymmetrical 1µM $[K^+]_{out}$ and 1 µM $[K^+]_{in}$. In asymmetrical conditions the ionic concentration was kept constant by replacing with Na^+ ions. In A, B, C n = 3 and error bars are s.e.m. **D.** Comparision of $\Delta\tau_{inact}$ at a difference of 50 mV driving force plotted against K^+ concentration.

4.3 Electrophysiological recording of KcsA WT, KcsA-Kv1.3 chimera and KcsA R64D

To understand the influence of different lipidic environments on potassium channel gating and to see which lipid binding amino acid has an influence on inactivation, KcsA WT, KcsA-Kv1.3 chimera and a point mutant of KcsA WT R64D were measured in different lipid mixtures. Inside out patch clamp on proteoliposomes in symmetrical 50 mM K+ solutions were used for all measurements. The channel was depolarized from 0 mV to +100 mV. Time constants, for activation and inactivation were measured together with steady state currents.

4.3.1 Purification of KcsA WT and gel analysis

KcsA WT expressed in *E.coli* containing the expression vector pQE 70 was purified and analysed by SDS PAGE and the concentration was measured. Heating the protein sample for

5 min still gave a band at a size of 60 KD (figure 4.9 A). The protein concentration measured at 260 nm was very low (0.6-0.8 mg of protein per litre of culture) which was not sufficient for electrophysiological recordings. If the protein KcsA WT was expressed in *E.coli* with expression vector pQE 32, the concentration was 1.5-1.7 mg of protein per litre of culture (optimum concentration for electrophysiological measurements). Analysis by SDS PAGE showed a protein band at a size of 17 KD (figure 4.10 B).

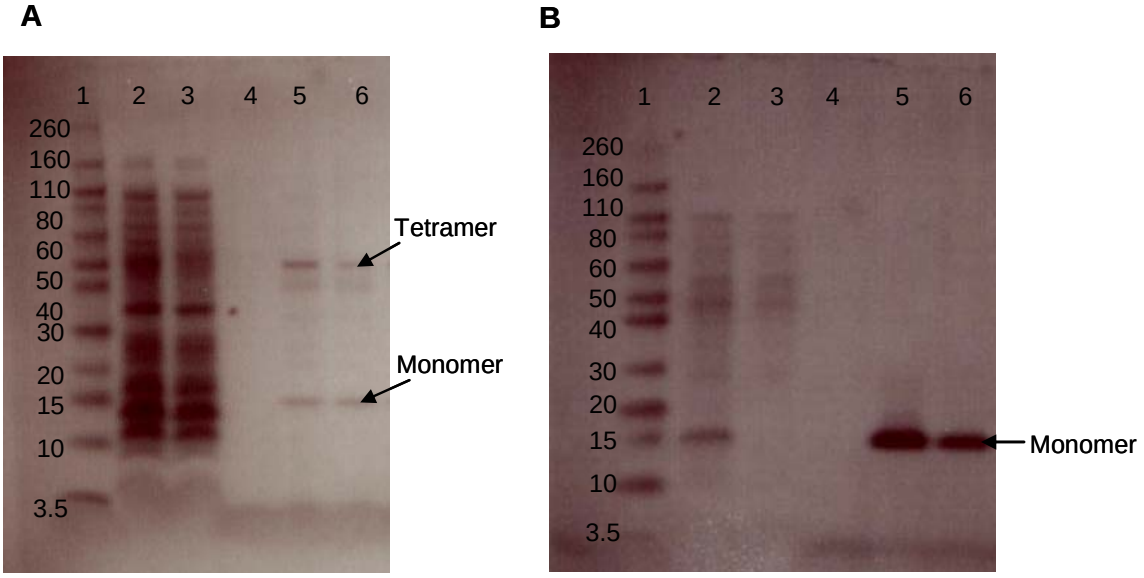

Figure 4.9: Gel image of KcsA WT in with different expression vectors.
A. Gel image showing the KcsA WT expressed using the expression vector pQE 70. The protein can be as a very faint band at both 60 KD and 17 KD in lanes 5 and 6. Lane 1 shows novex prestained marker in KD. Lane 2 is loaded with pellet from ultra centrigugation before purification where bands can be seen through the whole run lane 3 was the flowthrough from purification where as lane 4 was the washing step. **B.** Gel image of KcsA WT expressed using the expression vector pQE 32. The target protein band was observed at 17K D size. The lanes 1-4 are corresponding to that of 4.8 A.

4.3.2 Inactivation of KcsA WT and KcsA-Kv1.3 in asolectin lipid

KcsA WT and KcsA-Kv1.3 chimera differ by 13 amino acids in turret and pore helix (Legros et al., 2000). To investigate the lipid binding amino acid responsible for inactivation, KcsA WT current properties were compared to those of KcsA-Kv1.3. The channel was depolarized in pH 4.0 from 0 mV to +100 mV in symmetrical 50 mM K^+ solutions. Activation kinetics of KcsA WT was two fold faster (τ_{inact}=0.02±0.02 s, n=7, s.e.m, P=0.009) when compared to KcsA-Kv1.3. Inactivation kinetics displayed no significant difference between the KcsA WT and KcsA-Kv1.3 (figure 4.10 A). The steady state current amplitude was 12±2% (n=7 for KcsA WT and 4 for KcsA-Kv1.3, s.e.m) for of the peak amplitude for both WT and KcsA-Kv1.3 as shown in figure 4.10 B. No difference in inactivation was observed between KcsA WT and KcsA-Kv1.3 chimera in asolectin lipid.

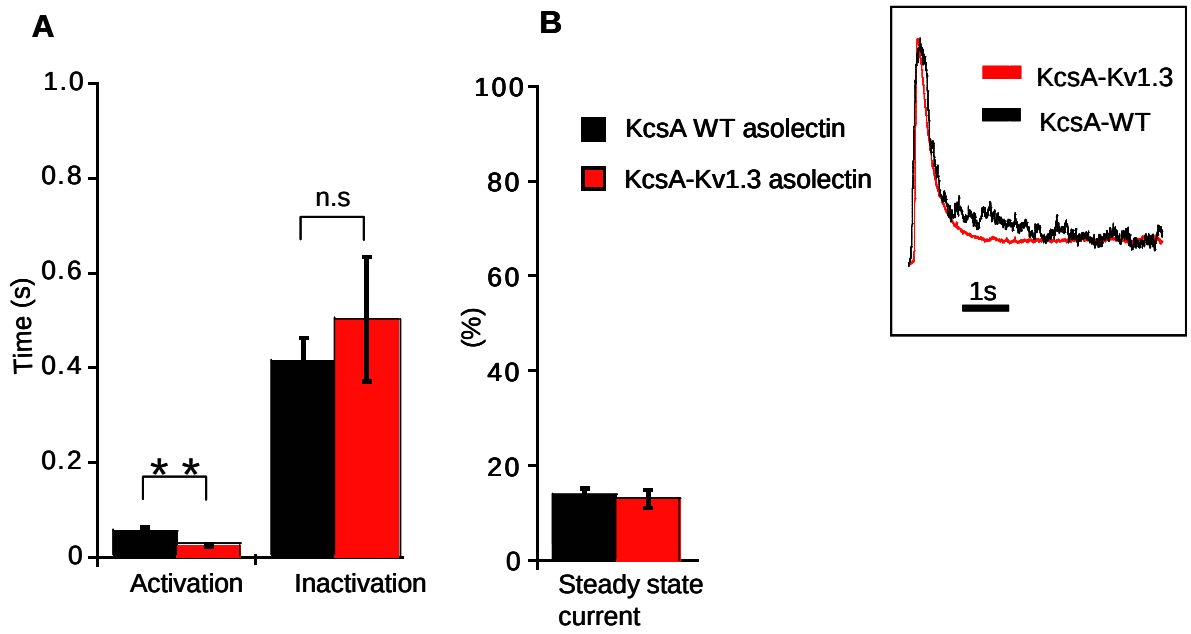

Figure 4.10:. KcsA WT and KcsA-Kv1.3 currents in asolectin lipid
A. Bar diagram comparing the activation and inactivation kinetics between KcsA WT and KcsA-Kv1.3. **B** Bar diagram comparing the steady state current. Error bars are s.e.m and n=5 for both the channels. **Inset:** comparision of current traces of KcsA WT and KcsA-Kv1.3 in asolectin proteoliposomes.

4.3.3 Influence of different lipids on KcsA WT

In the following experiments KcsA WT channel kinetics were measured in different lipids. Accordingly, KcsA WT was reconstituted into a combination of neutral and negatively charged phospholipids – DOPC: DOPG (7:3) and DOPC: DOPA (7:3) and the kinetics in symmetrical 50 mM K^+ solutions were compared with KcsA WT reconstituted into asolectin. There is a short delay in activation in phospholipids with neutral and negative charged combination when compared to asolectin which is a mixture of phospholipids with unknown charge. However, inactivation time courses were much faster in different phospholipid mixtures, τ_{inact}=0.07±0.02 s (n=4, s.e.m) but differ significantly from asolectin τ_{inact}=0.41±0.05 s (n=7, s.e.m, P=0.02, student T test) (figure 4.11 A). Steady state current amplitude was 4±0% (n=4, s.e.m) of the peak current amplitude and significantly different compared to asolectin (12±2%) (n=7, s.e.m, P=0.0004) (figure 4.11 B).

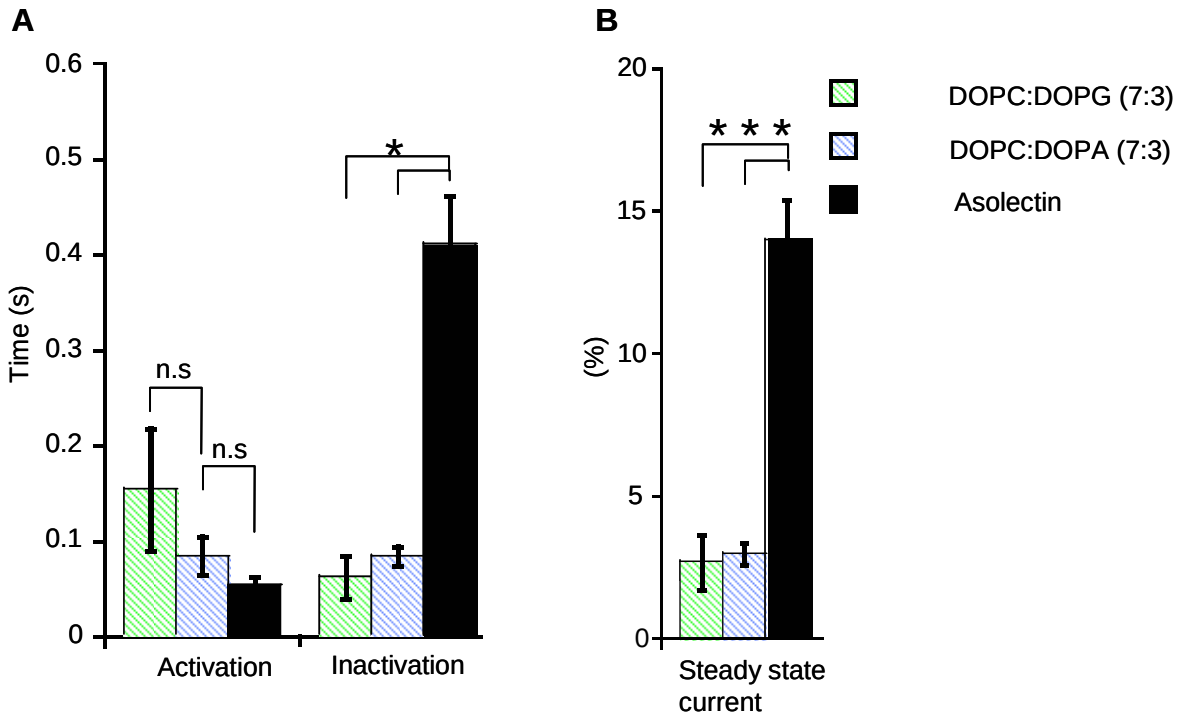

Figure 4.11: Influence of different phospholipids on KcsA WT currents.
A Bar diagram comparing the time constants for activation and inactivation in KcsA WT reconstituted into mixtures of different phospholipids. P=0.02 for inactivation. **B** Bar diagram comparing the steady state currents. P= 0.004. Error bars are s.e.m and n=5 for each.

4.3.4 Influence of different lipids on KcsA-Kv1.3 chimera

KcsA-Kv1.3 in different phospholipid mixtures DOPC: DOPG (7:3), DOPC: DOPA (7:3), and respectively DOPC: Cardiolipin (7:3) were measured in symmetrical 50 mM K^+ solutions. KcsA-Kv1.3 activation and inactivation kinetics in the different phospholipid mixtures were similar (figure 4.13 A). The only significant difference in KcsA-Kv1.3 inactivation was observed between asolectin (0.5±0.13 s) and DOPC: DOPG (7:3). However unlike in KcsA WT the time constants for inactivation were slightly different between different phospholipid mixtures with DOPG of 0.06±0.006 s, DOPA of 0.13±0.02 s and cardiolipin of 0.15±0.02 s (P=0.04, student T test, n=5 and s.e.m for each lipid mixture) (figure 4.12 A). The steady state current amplitude was lower in different lipid mixtures but a significant difference (P=0.04, student T test) was observed between DOPA (6±1.5%) (n=5 error bars=s.e.m) and asolectin (13±2%) (n=4, error bars=s.e.m) (figure 4.12 B).

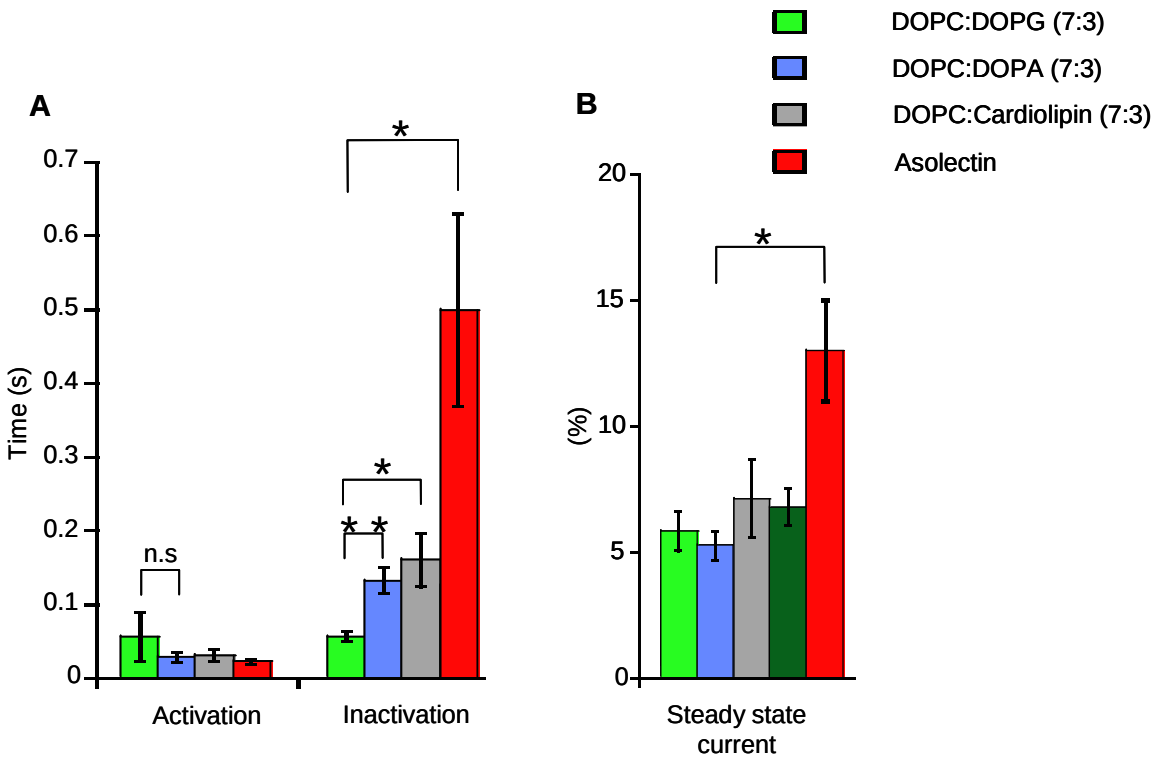

Figure 4.12: Influence of different phospholipids on KcsA-Kv1.3 currents.
A. Bar diagram showing the comparision of time constants of activation and inactivation of KcsA-Kv1.3 in different lipids. P value between DOPG and asolectin is 0.04 (student T test). **B.** Comparision of steady state currents. P value between DOPA and asolectin is 0.04. Error bars are s.e.m and n=5.

4.3.5 Effect of negative charge of the lipid on KcsA-Kv1.3 inactivation

According to the literature increasing POPG lipid in the membrane increases the open probability of the KcsA WT channel (Marius et al., 2008). Increasing the DOPG content in the mixture (DOPC: DOPG – 5:5 from 7:3) with respect to DOPC influenced inactivation of KcsA-Kv1.3. Activation kinetics showed no significant difference but channel inactivation was slower with τ_{inact}=0.06±0.006 s (n=7, s.e.m) for DOPC: DOPG (7:3) and τ_{inact}=0.15±0.02 s (n=7, s.e.m) for (5:5) (figure 4.13 A) indicating that negative charged lipid has an influence on inactivation. In contrast, steady state current showed no significant difference (P=0.19, student T test) upon increasing DOPG in the mixture (figure 4.13 B) (n=9 and s.e.m).

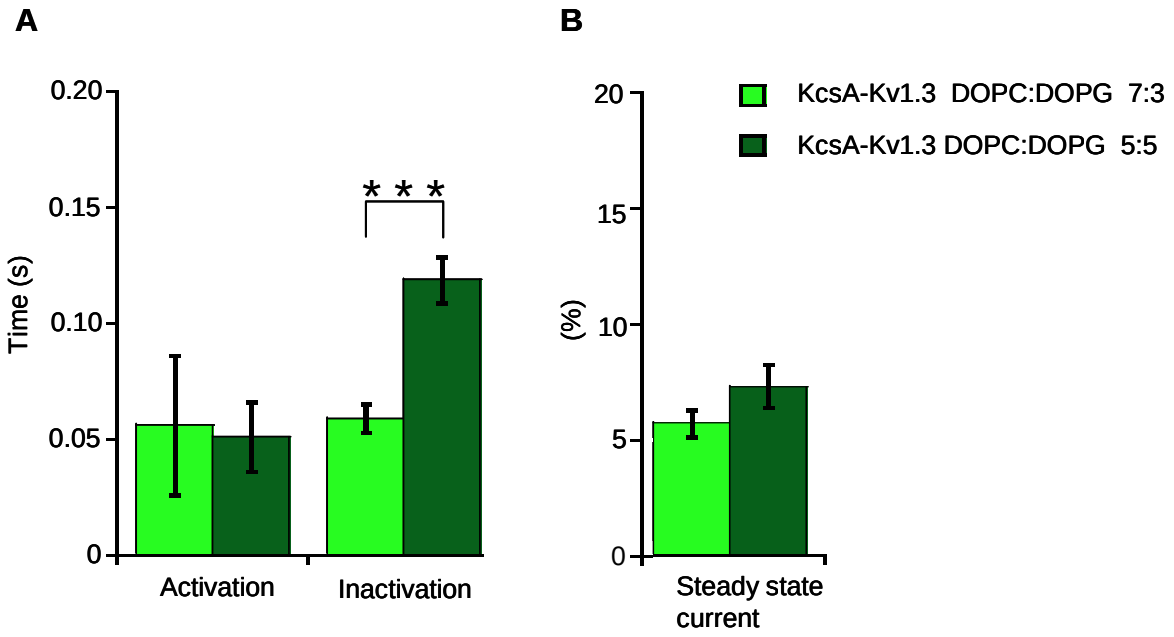

Figure 4.13: Influence of DOPG on KcsA-Kv1.3 inactivation.
A. Comparision of activation and inactivation time constants of KcsA-Kv1.3 in DOPC: DOPG (7:3) and (5:5). **B** Comparision of steady state currents. Error bars are s.e.m and n=9 for each.

4.4 Purification and electrophysiological analysis of KcsA R64D in asolectin

The amino acid R64 in KcsA has been proposed to be involved in direct lipid binding (Valiyaveetil et al., 2002). Inactivation and steady state gating properties of the KcsA R64D channel were investigated. KcsA R64D was expressed in pQE 32, purified and analysed by SDS PAGE as shown in Figure 4.15 A. Even expressed in pQE 32, the protein was observed as a tetramer after heating for 5 min before loading onto the gel. The point mutant was reconstituted into asolectin lipid. KcsA R64D activation and inactivation kinetics did not differ from KcsA WT and KcsA-Kv1.3 in asolectin (figure 4.14 B). The steady state current amplitude was increased significantly to 40 ± 2% (n=2 error bars = s.e.m) of the peak amplitude (figure 4.14 C).

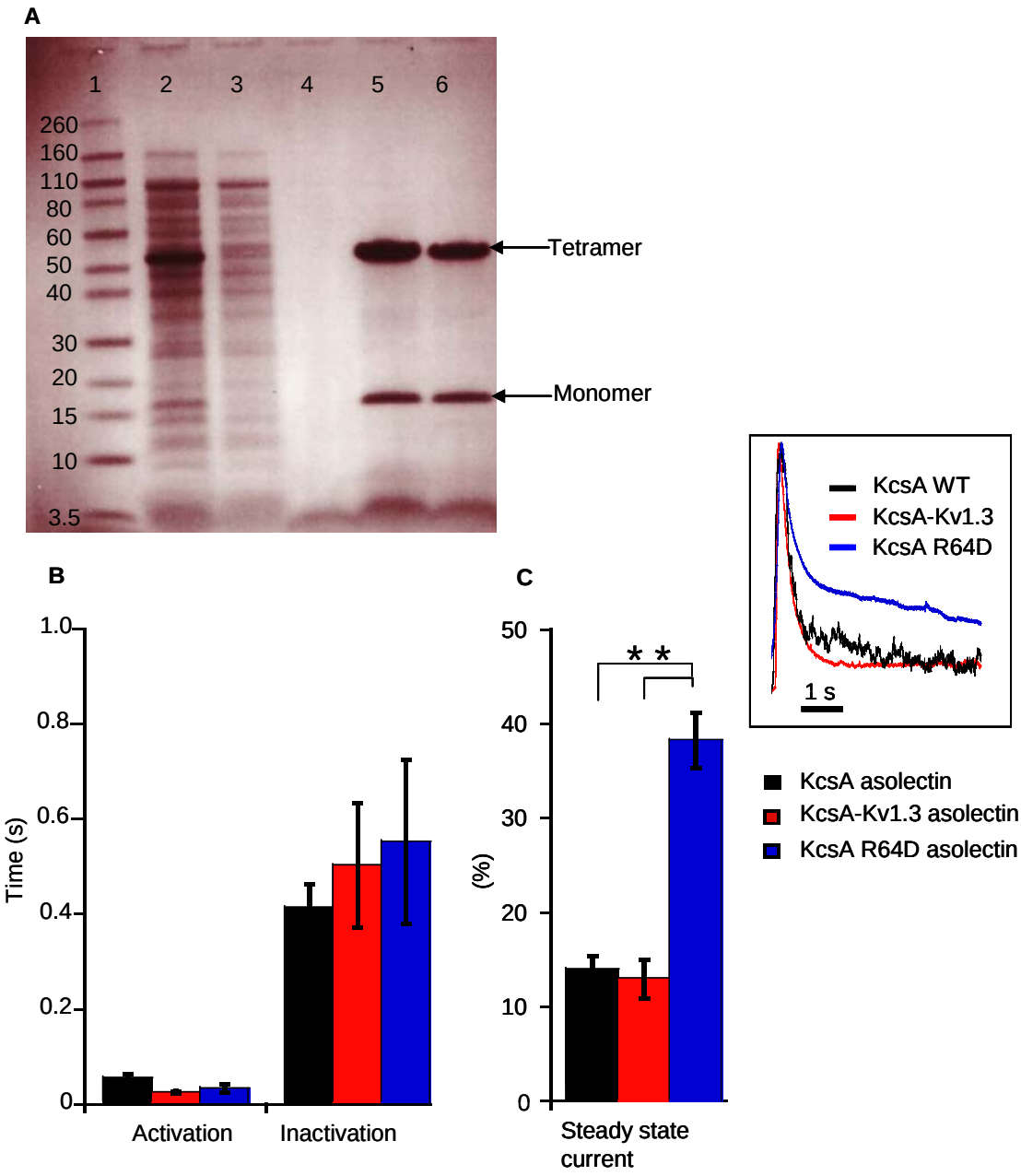

Figure 4.14: Gel image of KcsA R64D together with current properties comparing with KcsA WT and KcsA-Kv1.3.
A. Gel analysis of KcsA R64D expressed in pQE 32. The target protein was seen mostly at a size of 60 KD although a light band can be seen at 17 KD in lanes 5 and 6. Lane 1 - prestained marker in KD, lane 2 pellet from ultracentrifugation, lane 3 - Flowthrough, lane 4 – washout. **B.** Comparision of tau values of activation and inactivation of KcsA R64D with that of KcsA WT and KcsA-Kv1.3 in asolectin proteoliposomes. **C.** Comparision of steady state currents. P value=0.01. n=3 and error bars=s.e.m. **Inset:** comparision of KcsA WT, KcsA-Kv1.3 and KcsA R64D current traces.

5 Discussion

The purpose of this study is to functionally investigate inactivation gating of potassium channels in a structural context using solid state NMR and compare with previous X-ray structures (Doyle et al., 1998, Serdar et al., 2009, Thompson et al., 2009, Valiyaveetil et al., 2006, Zhou et al., 2001). Preference for NMR over X-ray crystallography is due to two reasons: X-ray crystals give a snapshot of particular state of an ion channel and the experimental conditions cannot be changed during the experiment. On the other hand experimental conditions can be changed during the experiment using NMR. X ray crystals of ion channels are made in detergent micelles and cannot be crystallized in physiological lipid environment whereas in NMR, channels incorporated into liposomes can be measured. This study of ion channel gating is an important aspect in ion channel physiology. Changes during activation and inactivation is important to study the gating properties. KcsA gating is sensitive to voltage, pH, lipid environment and K^+ ions. Inside out patch clamp of proteoliposomes containing KcsA- Kv1.3 and later KcsA WT and KcsA R64D was used to study the inactivation gating properties. To this end the protein was purified and reconstituted into proteoliposomes for electrophysiological analysis.

The KcsA-Kv1.3 chimera protein obtained by using expression vector pQE 32 (N- terminal histidine tag) showed a protein band size of 17 KD on SDS PAGE after heating for 5 min. Heating denatures the protein and the size is of a single KcsA-Kv1.3 subunit (monomer). The concentration was good enough for measuring macroscopic inactivating currents and was in nA range. The KcsA WT protein obtained by using expression vector pQE 70 (C- terminal histidine tag) showed a protein band size of 60 KD even after heating for 5 min which indicates a tetramer. Although relatively stable compared to pQE 32 expression vector, the concentration of the protein was too low that the inactivating currents were in the range of pA. Hence all of the proteins constructs used for the study were with expression vector pQE 32 vector. As reported earlier for KcsA WT (Cuello et al, 1998; Chakrapani et al, 2007a, 2007b), opening of the channel upon changing the intracellular pH to acidic from neutral pH confirm that KcsA-Kv1.3 is a proton gated channel and point to the presence of pH sensor at the inner helix bundle crossing. Inactivation after a short time similar to KcsA WT inactivation indicates that KcsA-Kv1.3 macroscopic inactivating currents are similar to KcsA WT (Ader et al., 2008). A simple and sequential scheme may describe gating of the KcsA channel. The scheme incorporates two gates within the conduction pathway of the KcsA channel: an activation gate and inactivation gate within the selectivity filter.

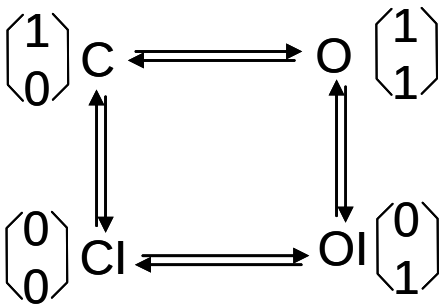

In the closed state (C) the activation (lower) gate is closed and the inactivation (upper) gate is open. Upon activation by protons the lower gate opens and ion conduction takes place. Opening the activation gate causes selectivity filter backbone reorientation due to coupling of gates, eventually leading to loss of potassium ions in binding sites 2 and 3 abrogating ion conduction. The inactivation gate closes (OI) while the lower gate stays open (Cuello et al., 2010). Finally in the closed inactivated state both the gates are closed. In this state the recovery from inactivation takes place. The open state and closed inactivated state are short lived and most of the time the channel resides in either closed state or open inactivated state. In both these states only either one of the gates are open and appears that opening of the lower gate leads to closure of the upper gate and lower gate closure favours opening of the upper gate.

5.1 Influence of permeant ions on KcsA-Kv1.3 inactivation

The influence of $[K^+]_{out}$ on selectivity filter stability and inactivation has been studied extensively (Zagotta and Aldrich, 1990, Demo and Yellen, 1991, Chakrapani et al, 2007b). How sequential gating activity of two gates in the pore is affected by the ion permeant ions is not understood and was studied. ssNMR and patch clamp electrophysiology was used to check the influence of K^+ on gating. A higher steady-state current and a slower inactivation at high $[K^+]_{out}$ when compared to low $[K^+]_{out}$ was observed for KcsA–Kv1.3 chimera. The same was reported in earlier studies with KcsA WT and Kv channels and is consistent with the idea that C-type inactivation is correlated with the collapse of a conductive selectivity-filter structure (Demo and Yellen, 1991; Baukrowitz and Yellen, 1995; Kiss and Korn, 1998; Ader et al, 2008). A K_D value of 0.9 mM was obtained for the sensitivity of KcsA–Kv1.3 inactivation to external $[K^+]$ as measured by steady-state current. Previous study found a similar value K_D of 0.43 mM for K^+ binding to the selectivity filter of KcsA (Lockless *et al*, 2007). In agreement with earlier reported outward-rectification properties of KcsA-mediated

currents, inactivation of KcsA–Kv1.3 inward current was essentially complete (Heginbotham et al, 1999; Chakrapani et al, 2007b). In addition, our electrophysiological experiments indicated that an internal high-affinity K^+-binding site with a K_D of 6.5 µM modulates KcsA–Kv1.3 activation gating. The overall ionic strength, which has been shown to influence channel open probability (Heginbotham et al, 1998), was kept constant in our experiments. Such a strategy also eliminates other side effects, for example related to surface potential or mechanical stability of the proteoliposome. Therefore, the observed K^+ effects on channel gating can be traced to K^+ itself. In electrophysiological experiments K^+-channel gating proceeds through an open-inactivated state, as established (Kurata and Fedida, 2006; Chakrapani et al, 2007a). ssNMR data showed a closed-conductive K^+-channel conformation at 50 mM [K^+] across the entire pH range of 4.0–7.5. In contrast, acidic pH in low K^+ induces a conformational change characterized by a stably opened activation gate (figure 5.1).

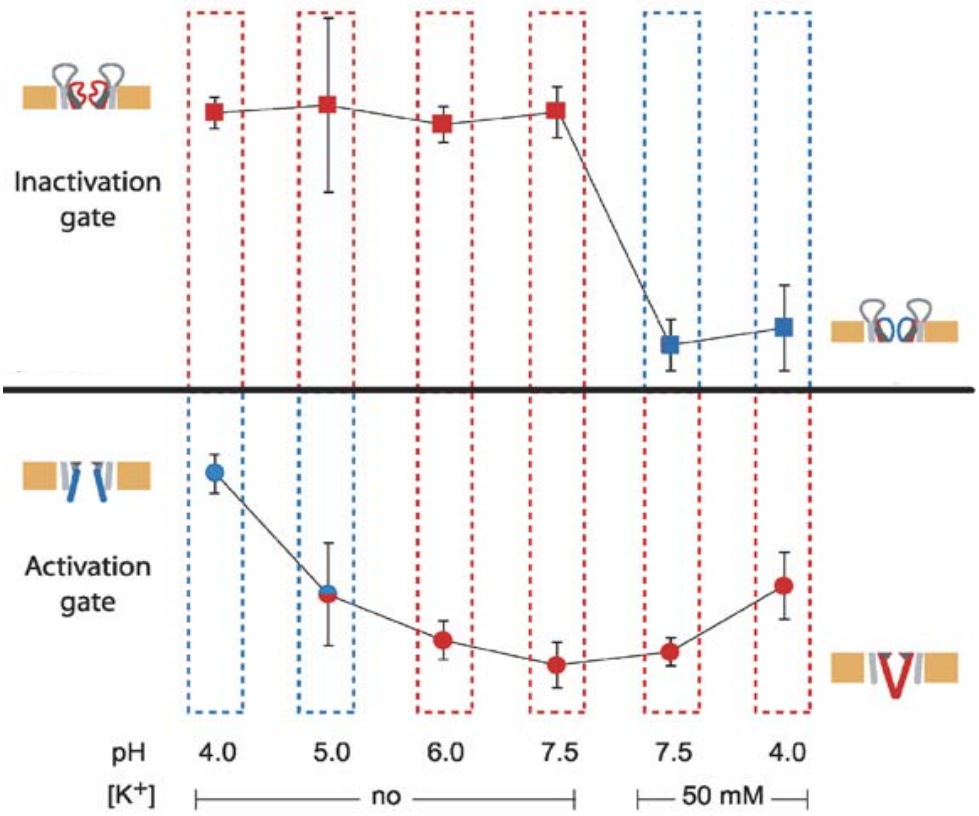

Figure 5.1: Conformations of activation and inactivation gate at different pH.
Activation gate is closed from pH 4.0-7.5 in 50mM K^+ (lower right) and opens when the potassium is removed or less (lower left). Inactivation gate is conductive at both pH 4.0 and 7.5 in presence of potassium but collapsed when potassium is less(Ader et al., 2009).

These ssNMR results had two important implications. First, acidic pH, which opens the KcsA–Kv1.3 channel, renders the selectivity-filter vulnerable to inactivation. Second, the probability of activation-gate opening at acidic pH is K^+ sensitive. The data show that the

prevailing KcsA–Kv1.3 conformation observed at pH 4.0 shifts from the open-collapsed (I) state to the closed-conductive (C) state of the channel in the presence of high millimolar K^+ concentrations (figure 5.2).

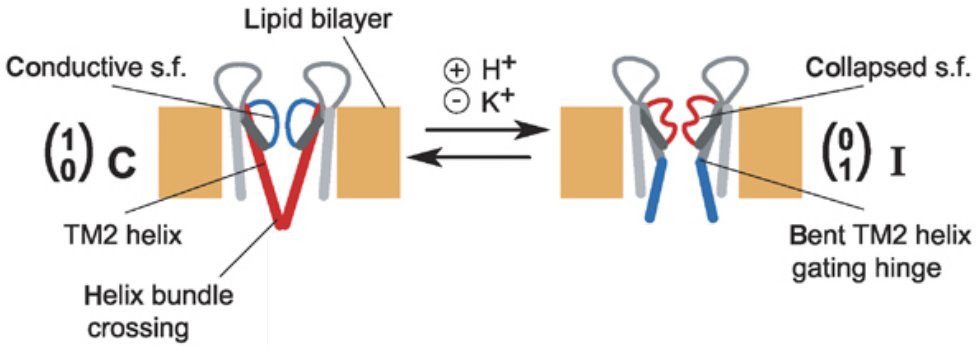

Figure 5.2: Cartoon representation of KcsA–Kv1.3 in a lipid bilayer setting.
Core elements of gating states are marked. The selectivity filter acts as inactivation gate and resides in conductive/open and collapsed/closed states. The activation gate is located in the TM2 helix of each subunit and gate opening is associated with a bent helix. H^+ induces gating transitions, whereas K^+ stabilizes the closed-conductive resting state of KcsA–Kv1.3(Ader et al., 2009).

This complements our electrophysiological studies on the K^+ dependency of KcsA-Kv1.3 channel inactivation and shows that both activation and inactivation gate of KcsA–Kv1.3 respond to changes in K^+ concentration at a structural level. The observation of closed conductive conformation of KcsA–Kv1.3 in asolectin liposomes even at pH 4.0 in millimolar (≥10 mM) K^+ concentrations is due to the absence of transmembrane voltage. The data shows that KcsA–Kv1.3-channel inactivation is over 100-fold more sensitive to $[K^+]_{in}$ than to $[K^+]_{out}$. It suggested that occupation of an internal K^+ binding site presumably in the water filled cavity below the selectivity filter and external binding site towards the extracellular end of the selectivity filter modulates KcsA–Kv1.3-channel gating. This implies that equilibria between activated and inactivated channel states, which are influenced by changes in $[K^+]_{in}$ and $[K^+]_{out}$, are correlated with K^+-sensitive conformational rearrangements in the KcsA–Kv1.3 channel. However recovery from inactivation is unaffected in neither different $[K^+]_{out}$ nor in different $[K^+]_{in}$ and it was known that recovery from inactivation occurs only when the activation gate is closed. Hence when the activation gate is closed both $[K^+]_{out}$ and $[K^+]_{in}$ do not influence recovery from inactivation (Ader et al., 2009).

As reported previously, that Rb^+ as the permeant ion slows C-type inactivation due to longer residual time in the selectivity filter (Lopez Barneo et al., 1993; Shahidullah and Covarrubias, 2003), inactivation of KcsA-Kv1.3 chimera is slowed down drastically in symmetrical Rb^+ mediated outward currents compared to symmetrical K^+ mediated outward currents. In inward

currents inactivation is similar in both Rb^+ currents and K^+ currents. This can be explained by the fact that during KcsA WT inactivation loss of ions at binding site 2 and 3 leads to narrowing of selectivity filter at binding site 1 and expansion at site 4 occurs (Cuello et al., 2010a) (figure 5.3).

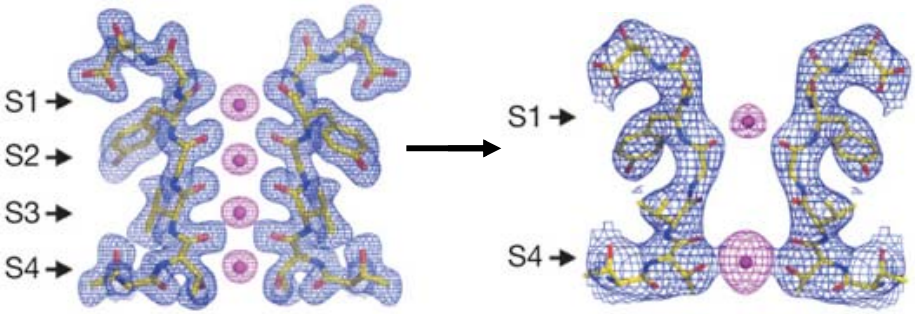

Figure 5.3. Crystal structure of KcsA selectivity filter in different conformations.
In closed conductive conformation ions are present in all the four binding sites (left). Ions are lost at binding sites 2 and 3 coupled with narrowing of filter at site 1 and expansion at site 4 in open inactivated state (Cuello et al., 2010a).

The assumption is, in outward currents occupancy of bigger size Rb^+ ions at the narrow part of the filter at position 1 slow KcsA inactivation. Due to the expansion at site 4, occupancy of ions at site 4 is independent of the size of the permeant ion and hence Rb^+ mediated inactivation in inward currents is similar to K^+ currents. Recovery from inactivation in Rb^+ mediated outward and inward currents are unaffected and similar to K^+ mediated recovery from inactivation and can be due to the same reason that when the activation is closed the permeant ions does not have an influence on recovery from inactivation.

To investigate whether the influence of $[K^+]_{out}$ and $[K^+]_{in}$ on KcsA-Kv1.3 inactivation is due to the driving force in response to K^+ solutions or due to voltage, inactivation was measured at different voltages. Formation of a bell shaped curve in symmetrical 150 mM K^+ solutions and 20 mM and 1µM asymmetrical $[K^+]_{out}$ and $[K^+]_{in}$ revealed that KcsA-Kv1.3 inactivation is voltage independent. Inactivation is said to be voltage dependent when the time constants for inactivation increase with increased voltage (Cordero Morales et al., 2006b). This is due to, more open channels at higher voltages are harder to inactivate. Different $\Delta\tau_{inact}$ values in different K^+ at similar delta driving force suggest that although a small dependence on driving force the inactivation is due to differences in K^+ concentrations. Hence it can be summarized that the inactivation of KcsA-Kv1.3 is influenced by differences in K^+ and inactivation at different voltages are due to differences in driving force but not due to different voltages.

5.2 Influence of lipid environment on K^+ channel inactivation

Influence of lipid environment on KcsA function has been extensively studied (Valiyaveetil et al., 2002, Marius et al., 2008, Alvis et al., 2003) but the influence of different lipidic environment on KcsA inactivation has been not well studied. No change in the inactivation kinetics and steady state current amplitude between KcsA WT and KcsA-Kv1.3 in asolectin lipid indicated that asolectin has the same influence on inactivation in both these channels. Asolectin is a mixture of phospholipids with 25% of phosphatidyl choline. To see which phospholipid component has an influence on inactivation, current properties KcsA WT and KcsA-Kv1.3 in combination of neutral and different anionic phospholipids were investigated. In combination of neutral and negative charged phospholipids DOPC: DOPG (7:3) and DOPC: DOPA (7:3) KcsA WT inactivated fast and complete. Compared to asolectin the data indicated that these combination of phospholipids accelerate KcsA WT the inactivation. Similar inactivation time constants and steady state current amplitudes of KcsA in the two lipid mixtures indicate that packing or interaction of these lipids to the channel is similar. Similar results were obtained for KcsA-Kv1.3 in these lipid combinations. In addition the combination DOPC: Cardiolipin (7:3) generated similar results. It is likely a phospholipid combination apart from these lipids in asolectin slows inactivation. Rb^+ flux experiments (Valiyaveetil et al., 2002) showed that combination of PE: PG increased the uptake of Rb^+ in KcsA compared to PE: PC. Possibly the interaction of the neutral lipid DOPC with the KcsA channel was responsible for slowing inactivation. Previous studies showed that increasing PG content in the membrane increases the open probability of KcsA WT (Marius et al., 2008). A comparable effect was observed for KcsA-Kv1.3, where upon increasing the amount of PG relative to PC (DOPC: DOPG-5:5) KcsA-Kv1.3 inactivation slowed and steady state current increased.

Mutational studies showed that R64A slows inactivation (Cordero morales et al., 2006b) and lipids used in KcsA structure and refolding studies (Deol et al., 2005, Valiyaveetil et al., 2002). Lipid binds to R64 from one subunit with its head group and to R89 from the adjacent subunit with its lipid tail. This interaction may explain why mutation of R64 to A64 in KcsA WT drastically slowed the inactivation process. A point mutation of R64 to D64 was made and current properties were investigated. The increased steady state current of point mutant KcsA R64D in indicated that this amino acid alone has an influence on inactivation. It is likely a local effect. Although the lipid binding amino acid residue R 64 is D 64 in KcsA-Kv1.3 but together with 12 other different amino acids from Kv1.3 at the extracellular end.

The effect of D64 on inactivation was minimized by the presence of interaction of these 12 other amino acids from Kv1.3 and hence the inactivation of KcsA-Kv1.3 is similar to KcsA WT. Possibly, the negatively charge lipid binds between positively charged R64 and 89 (figure 5.4) of the protein thereby neutralizing the charge (Vales and Raja, 2010).

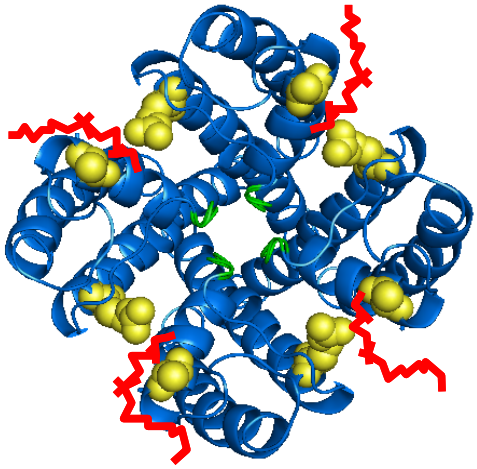

Figure 5.4: Cartoon representation of KcsA WT with the lipid binding to lipid binding amino acids.
Lipid binding amino acids are indicated as yellow spheres. The negatively charged lipid molecule indicated as red lines is assumed to be bound between this lipid molecules

Then, mutation of R64 to negatively charged D64 or A64 would lead to a loss of charge neutralization and eventually disturb packing of protein and lipid. This would be associated with a conformational change that slows inactivation.

6 Conclusion

It was shown that the KcsA-Kv1.3 K^+ channel is activated by intracellular protons and undergoes macroscopic inactivation like KcsA WT. KcsA-Kv1.3 inactivation was sensitive to extracellular K^+ with a K_D value of 0.9 mM and to intracellular K^+ with a K_D value of 6.5 µM. The results indicated that sequential gating activity of KcsA-Kv1.3 is influenced by different extracellular and intracellular K^+. Inactivation kinetics was 100 fold more sensitive to intracellular K^+ than extracellular K^+. As known from previous studies (Shahidullah et al., 2003), it was shown that Rb^+ as a permeant ion slows inactivation of KcsA-Kv1.3 outward currents. Rb^+ had no influence on inward current kinetics. The time constants obtained by measuring inactivation at different voltages suggest that differences in K^+ dependent inactivation observed at different voltages were due to differences in driving force and not to differences in voltage. Inactivation of KcsA WT and KcsA-Kv1.3 was similar in asolectin. Measurement of KcsA WT and KcsA-Kv1.3 currents in mixtures of different neutral and negative charged phospholipids resulted in faster inactivation when compared to asolectin. The results suggest that neutral phospholipid in the mixture is responsible. Increase of steady state current in KcsA R64D indicates that mutation of R64 affects inactivation and suggest that R64 is an important interaction site for the lipid head group.

7 References

- Ader C, Schneider R, Hornig S, Velisetty P, Wilson EM, Lange A, Giller K, Ohmert I, Martin-Eauclaire MF, Trauner D, Becker S, Pongs O, Baldus M. (2008) A structural link between inactivation and block of a K+ channel, Nat Struct Mol Biol. 15, 605-12
- Ader C, Schneider R, Hornig S, Velisetty P, Vardanyan V, Giller K, Ohmert I, Becker S, Pongs O, Baldus M. (2009) Coupling of activation and inactivation gate in a K+-channel: potassium and ligand sensitivity, EMBO J., 28, 2825-34.
- Aldrich RW. (2001) Fifty years of inactivation, Nature, 411, 643-4
- Alvis SJ, Williamson IM, East JM, Lee AG. (2003) Interactions of anionic phospholipids and phosphatidylethanolamine with the potassium channel KcsA, Biophys J, 85, 3828-38.
- Armstrong CM. (1969). Inactivation of the potassium conductance and related phenomena caused by quaternary ammonium ion injection in squid axons. J Gen Physiol, 54, 553-75.
- Baukrowitz T, Yellen G. (1995) Modulation of K^+ current by frequency and external $[K^+]$: a tale of two inactivation mechanisms, Neuron, 15, 951–960.
- Chakrapani S, Cordero-Morales JF, Perozo E. (2007a) A quantitative description of KcsA gating I: macroscopic currents, J Gen Physiol, 130, 465-78
- Chakrapani S, Cordero-Morales JF, Perozo E. (2007b) A quantitative description of KcsA gating II: single-channel currents, J Gen Physiol, 130, 479-96.
- Choi KL, Aldrich RW, Yellen G. (1991) Tetraethylammonium blockade distinguishes two inactivation mechanisms in voltage-activated K+ channels, Proc Natl Acad Sci U S A., 88, 5092-5.
- Connor JA, Stevens CF. (1971) Inward and delayed outward membrane currents in isolated neural somata under voltage clamp, J Physiol, 213, 1-19.
- Cordero-Morales JF, Cuello LG, Perozo E. (2006a) Voltage-dependent gating at the KcsA selectivity filter, Nat Struct Mol Biol, 13, 319-22.
- Cordero-Morales JF, Cuello LG, Zhao Y, Jogini V, Cortes DM, Roux B, Perozo E. (2006b) Molecular determinants of gating at the potassium-channel selectivity filter, Nat Struct Mol Biol, 13, 311-8.
- Cuello LG, Romero JG, Cortes DM, Perozo E. (1998) pH-dependent gating in the Streptomyces lividans K+ channel, Biochemistry, 37, 3229-36.

- Cuello LG, Cortes DM, Jogini V, Sompornpisut A, Perozo E. (2010) A molecular mechanism for proton-dependent gating in KcsA, FEBS Lett, 584, 1126-32.
- Cuello LG, Jogini V, Cortes DM, Perozo E. (2010a) Structural mechanism of C-type inactivation in K(+) channels, Nature, 466, 203-8.
- Cuello LG, Jogini V, Cortes DM, Pan AC, Gagnon DG, Dalmas O, Cordero-Morales JF, Chakrapani S, Roux B, Perozo E. (2010b) Structural basis for the coupling between activation and inactivation gates in K(+) channels, Nature, 466, 272-5.
- Demo SD, Yellen G. (1991) The inactivation gate of the Shaker K^+ channel behaves like an open-channel blocker, Neuron 7, 743–753
- Deol SS, Domene C, Bond PJ, Sansom MS. (2006) Anionic phospholipid interactions with the potassium channel KcsA: simulation studies, Biophys J, 90, 822-30.
- Doyle DA, Morais Cabral J, Pfuetzner RA, Kuo A, Gulbis JM, Cohen SL, Chait BT, MacKinnon R. (1998) The structure of the potassium channel: molecular basis of K+ conduction and selectivity, Science, 280, 69-77.
- Gao L, Mi X, Paajanen V, Wang K, Fan Z. (2005) Activation-coupled inactivation in the bacterial potassium channel KcsA, Proc Natl Acad Sci, 102, 17630-5.
- Grissmer S, Cahalan M. (1989) TEA prevents inactivation while blocking open K+ channels in human T lymphocytes, Biophys J, 55, 203-6.
- Heginbotham L, Kolmakova-Partensky L, Miller C. (1998) Functional reconstitution of a prokaryotic K+ channel, J Gen Physiol, 111, 741-9.
- Heginbotham L, LeMasurier M, Kolmakova-Partensky L, Miller C. (1999) Single streptomyces lividans K(+) channels: functional asymmetries and sidedness of proton activation, J Gen Physiol, 114, 551-60
- HILLE, B. (2001). Ion Channels of Exitable Membranes. *Sutherland, Massachusetts:*
- *Sinauer Associates*, 3rd. Edition
- Hoshi T, Zagotta WN, Aldrich RW. (1990) Biophysical and molecular mechanisms of Shaker potassium channel inactivation, Science, 250, 533-8.
- Jiang Y, Lee A, Chen J, Cadene M, Chait BT, MacKinnon R. (2002) The open pore conformation of potassium channels, Nature, 417, 523-6.
- Kiss L, Korn SJ. (1998) Modulation of C-type inactivation by K^+ at the potassium channel selectivity filter, Biophys J, 74, 1840–1849.

- Kurata HT, Doerksen KW, Eldstrom JR, Rezazadeh S, Fedida D. (2005) Separation of P/C- and U-type inactivation pathways in Kv1.5 potassium channels, J Physiol, 568, 31-46.
- Kurata HT, Fedida D. (2006) A structural interpretation of voltage-gated potassium channel inactivation, Prog Biophys Mol Biol, 92, 185-208.
- Lange A, Giller K, Hornig S, Martin-Eauclaire MF, Pongs O, Becker S, Baldus M. (2006) Toxin-induced conformational changes in a potassium channel revealed by solid-state NMR, Nature, 440, 959-62.
- Legros C, Pollmann V, Knaus HG, Farrell AM, Darbon H, Bougis PE, Martin-Eauclaire MF, Pongs O. (2000) Generating a high affinity scorpion toxin receptor in KcsA-Kv1.3 chimeric potassium channels, J Biol Chem, 275, 16918-24.
- Legros C, Schulze C, Garcia ML, Bougis PE, Martin-Eauclaire MF, Pongs O. (2002) Engineering-specific pharmacological binding sites for peptidyl inhibitors of potassium channels into KcsA, Biochemistry, 41, 15369-75
- Liu Y, Jurman ME, Yellen G. (1996) Dynamic rearrangement of the outer mouth of a K+ channel during gating, Neuron, 16, 859-67.
- Lockless SW, Zhou M, MacKinnon R. (2007) Structural and thermodynamic properties of selective ion binding in a K^+ channel, PLoS Biol, 5, e121.
- Long SB, Campbell EB, Mackinnon R. (2005) Voltage sensor of Kv1.2: structural basis of electromechanical coupling, Science, 309,903-8.
- López-Barneo J, Hoshi T, Heinemann SH, Aldrich RW. (1993) Effects of external cations and mutations in the pore region on C-type inactivation of Shaker potassium channels, Receptors Channels, 1, 61-71.
- Marius P, Zagnoni M, Sandison ME, East JM, Morgan H, Lee AG. (2008) Binding of anionic lipids to at least three nonannular sites on the potassium channel KcsA is required for channel opening, Biophys J, 94, 1689-98.
- Morais-Cabral JH, Zhou Y, MacKinnon R. (2001) Energetic optimization of ion conduction rate by the K+ selectivity filter, Nature, 414, 37-42.
- Murrell-Lagnado RD, Aldrich RW. (1993) Energetics of Shaker K channels block by inactivation peptides, J Gen Physiol, 102, 977-1003.
- Panyi G, Sheng Z, Deutsch C. (1995) C-type inactivation of a voltage-gated K+ channel occurs by a cooperative mechanism, Biophys J, 69, 896-903.

- Rasmusson RL, Morales MJ, Castellino RC, Zhang Y, Campbell DL, Strauss HC. (1995) C-type inactivation controls recovery in a fast inactivating cardiac K+ channel (Kv1.4) expressed in Xenopus oocytes, J Physiol, 489, 709-21.
- Uysal S, Vásquez V, Tereshko V, Esaki K, Fellouse FA, Sidhu SS, Koide S, Perozo E, Kossiakoff A.(2009) Crystal structure of full-length KcsA in its closed conformation. Proc Natl Acad Sci, 106, 6644-9.
- Shahidullah M, Covarrubias M. (2003) The link between ion permeation and inactivation gating of Kv4 potassium channels, Biophys J, 84, 928-41.
- Thompson AN, Posson DJ, Parsa PV, Nimigean CM. (2008) Molecular mechanism of pH sensing in KcsA potassium channels, Proc Natl Acad Sci, 105, 6900-5.
- Thompson AN, Kim I, Panosian TD, Iverson TM, Allen TW, Nimigean CM. (2009) Mechanism of potassium-channel selectivity revealed by $Na(^{+})$ and $Li(^{+})$ binding sites within the KcsA pore, Nat Struct Mol Biol, 16,1317-24.
- Valiyaveetil FI, Zhou Y, MacKinnon R. (2002) Lipids in the structure, folding, and function of the KcsA K+ channel, Biochemistry, 41,10771-7.
- Valiyaveetil FI, Sekedat M, MacKinnon R, Muir TW. (2006) Structural and functional consequences of an amide-to-ester substitution in the selectivity filter of a potassium channel. J Am Chem Soc, 128, 11591-9.
- Williamson IM, Alvis SJ, East JM, Lee AG. (2002) Interactions of phospholipids with the potassium channel KcsA, Biophys J, 83, 2026-38.
- Yellen G, Sodickson D, Chen TY, Jurman ME. (1994) An engineered cysteine in the external mouth of a K+ channel allows inactivation to be modulated by metal binding, Biophys J, 66, 1068-75.
- Yellen G. (2002) The voltage-gated potassium channels and their relatives, Nature, 419, 35-42.
- Zagotta WN, Aldrich RW. (1990) Voltage-dependent gating of Shaker A-type potassium channels in Drosophila muscle, J Gen Physiol 95, 29–60.
- Zakharian E, Reusch RN. (2004) Streptomyces lividans potassium channel KcsA is regulated by the potassium electrochemical gradient, Biochem Biophys Res Commun, 316, 429-36.
- Zhou Y, Morais-Cabral JH, Kaufman A, MacKinnon R. (2001) Chemistry of ion coordination and hydration revealed by a K+ channel-Fab complex at 2.0 A resolution, Nature, 414, 43-8.

8 Appendix

8.1 Abbreviations

Å	Angstrom
~	Approximately
C	closed
$CaCl_2$	Calcium Chloride
CI	closed inactivated
C-Terminus	Carboxy-terminus
DEPC	Diethyl pyrocarbonate
DOPA	1,2 Dioleoyl-*sn*- Glycero-3-phsophate (Mononsodium salt)
DOPC	1,2 Dioleoyl-*sn*- Glycero-3-phsopho choline
DOPE	1,2 Dioleoyl-*sn*- Glycero-3-phsophoethanolamine
DOPG	1,2 Dioleoyl-*sn*- Glycero-3-((phospho-rac-(1-glycerol)) (sodium salt)
DM	n-Decyl-ß-D-maltopyranoside
DMSO	Dimethylsulfoxide
DNA	Deoxyribonucleic acid
E. coli	*Escherichia coli*
EDTA	Ethylenediaminetetraacetic acid
et al.	et alii
exp	Exponent
°C	Degree Celsius
g	Centrifugal force
h	Hour
H+	Hydrogen ion
H-bonds	Hydrogen bonds
HEPES	2-[4-(2-Hydroxyethyl)-1-piperazinyl]-ethane-sulfonicacid
Hz	Hertz
I	Current
I_{norm}	Normalized current
I_{max}	Maximum current
I_{ss}	Steady state current
i.e.,	that is

In	Inside
IPTG	Iso propyl β-D-1-thio galactoside
K^+	Potassium ion
$[K^+]_{out}$	Extracellular potassium concentration
$[K^+]_{in}$	Intracellular potassium concentration
KCl	Potassium chloride
KcsA	Potassium channel from *Streptomyces lividans*
KD	Kilo Dalton
K_D	Dissociation constant
KHz	Kilohertz
Kv	Voltage gated potassium channel
Kv1	*Shaker*-related potassium channel
<	Less than
µA	Microampere
µg	Microgram
µL	Microliter
µM	Micromolar
µS	Microsecond
mg	Milligram
mL	Milliliter
mM	Millimolar
ms	Millisecond
mV	Millivolt
min	Minutes
MOPS	3-(N-Morpholino)-propanesulfonic acid
MnCl2	Manganese chloride
MW	Molecular weight
n, *n*	Number
nA	Nanoampere
ng	Nanogram
nM	Nanomolar
Na^+	Sodium ion
NaCl	Sodium chloride
NaH_2Po_4	Sodium dihydrogen phosphate

Na_2HPo_4	di sodium hydrogen phosphate
Ni-NTA	Nickel NTA
Na-P	Sodium phosphate
ssNMR	Solid state *Nuclear Magnetic Resonance*
norm	Normalized
N-Terminus	Amino-Terminus
O	*open*
OI	open inactivated
O.D	Optical density
Out	Outside
%	Percent
P	Probability
pA	Picoampere
pH	Negative logarithm of H+ concentration
PiPES	Piperazine-N,N′-bis(2-ethanesulfonic acid)
PLL	Poly-l-lysine hydrobromide
Po	Open probability
Rb^+	Rubidium ion
RbCl	Rubidium chloride
RPM	Revolutions per minute
s	Seconds
S1-S6	Transmembrane segment 1-6
S1-S4	Voltage sensing domain 1-4
SDS PAGE	Sodium dodecyl sulphate poly acrylamide gel electrophoresis
s.e.m.	*Sstandard error of the mean*, standard error
SF	Selectivity filter
SOB	Super Optimal Broth
T	Temperature (Kelvin), T-conformation
t	Time
τ	tau, time constant
TEA^+	Tetraethylammonium
TM	Transmembrane segment
v/v	volume/volume
V	Voltage

w/w	weight/weight
WT	Wild type

8.2 Expression vectors and clones

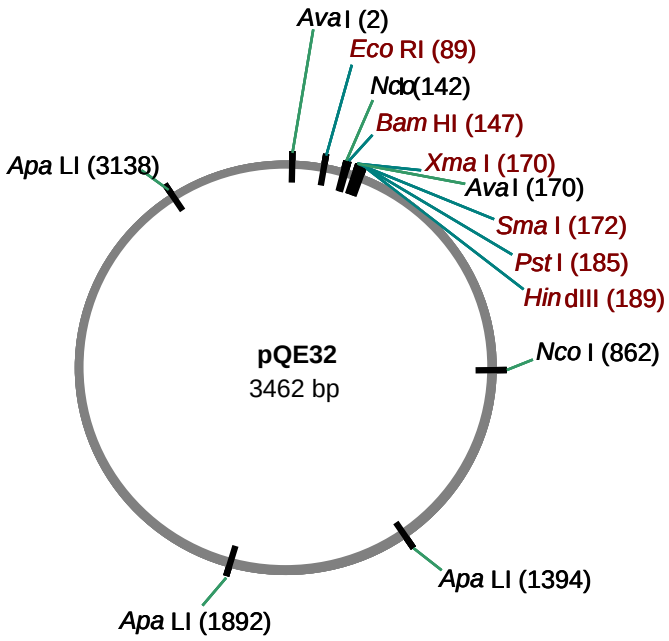

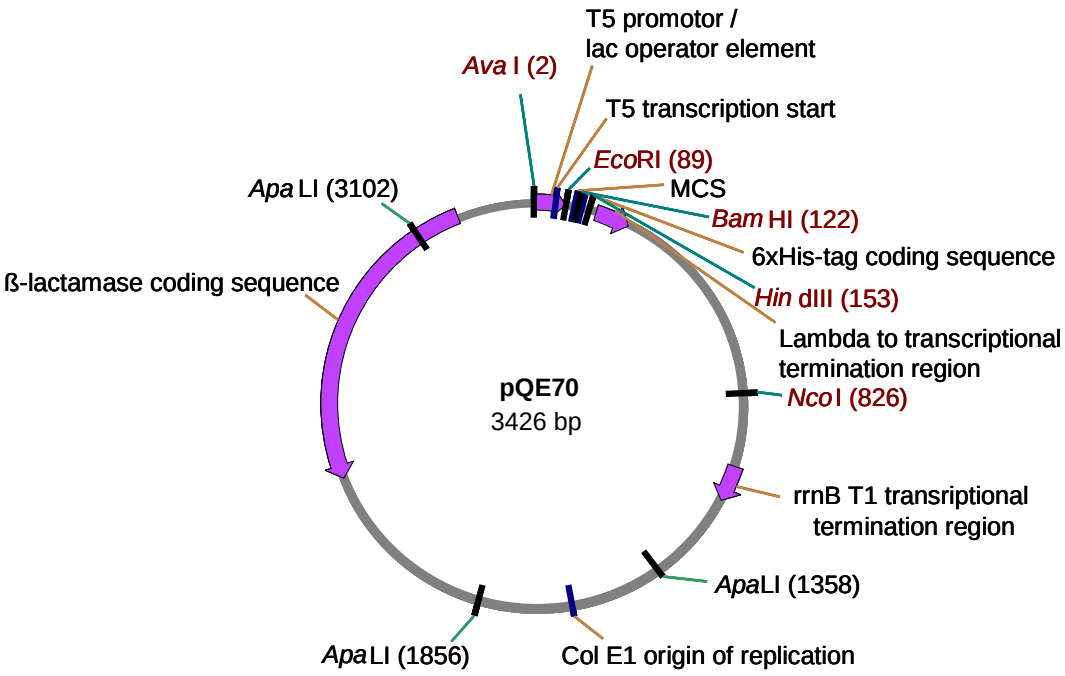

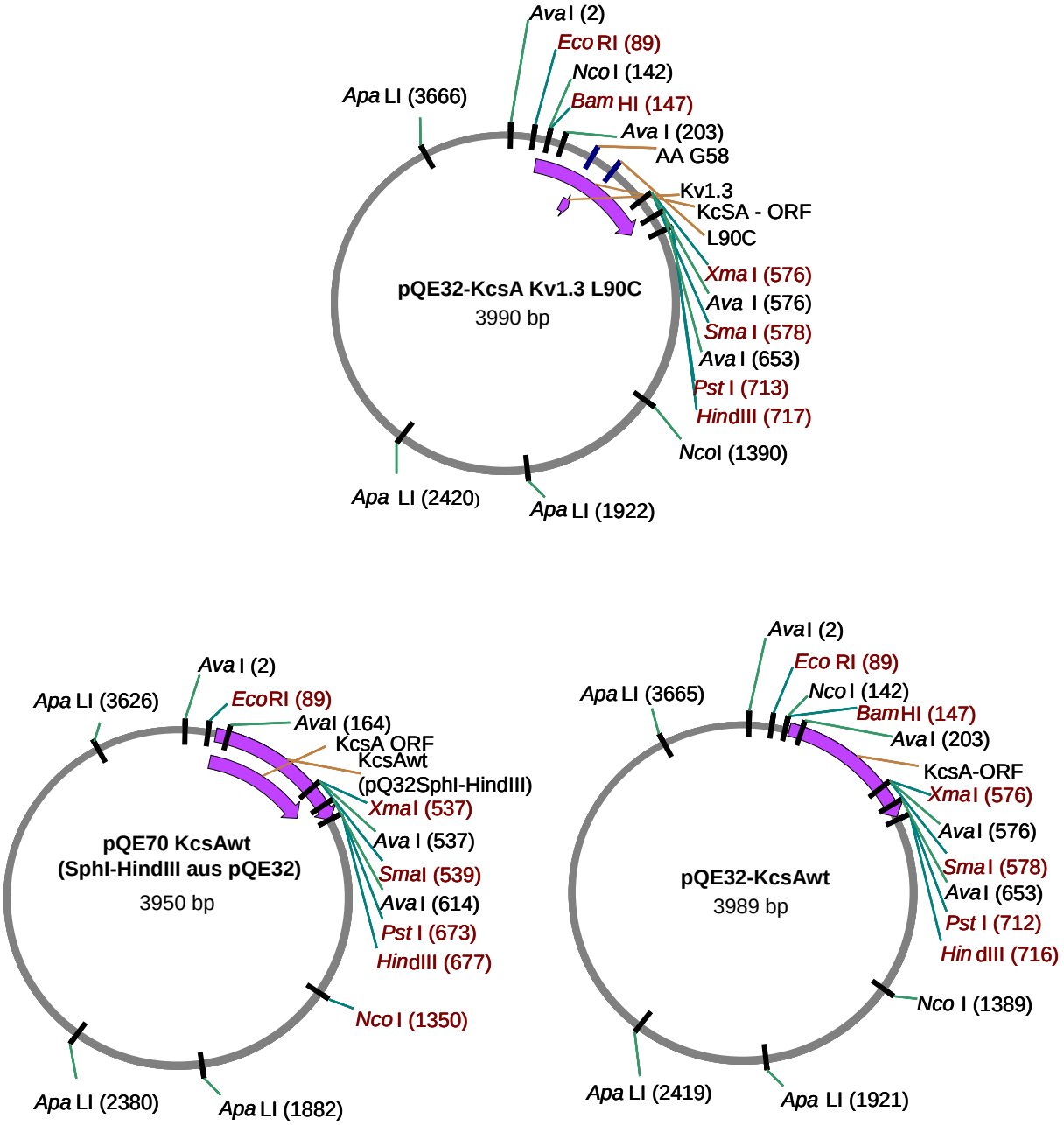
AvaI (2)
EcoRI (89)
NcoI (142)
BamHI (147)
AvaI (203)
AA G58
Kv1.3
KcSA - ORF
L90C
XmaI (576)
AvaI (576)
SmaI (578)
AvaI (653)
PstI (713)
HindIII (717)
NcoI (1390)
ApaLI (1922)
ApaLI (2420)
ApaLI (3666)
pQE32-KcsA Kv1.3 L90C
3990 bp
AvaI (2)
EcoRI (89)
AvaI (164)
KcsA ORF
KcsAwt
(pQ32SphI-HindIII)
XmaI (537)
AvaI (537)
SmaI (539)
AvaI (614)
PstI (673)
HindIII (677)
NcoI (1350)
ApaLI (1882)
ApaLI (2380)
ApaLI (3626)
pQE70 KcsAwt
(SphI-HindIII aus pQE32)
3950 bp
AvaI (2)
EcoRI (89)
NcoI (142)
BamHI (147)
AvaI (203)
KcsA-ORF
XmaI (576)
AvaI (576)
SmaI (578)
AvaI (653)
PstI (712)
HindIII (716)
NcoI (1389)
ApaLI (1921)
ApaLI (2419)
ApaLI (3665)
pQE32-KcsAwt
3989 bp

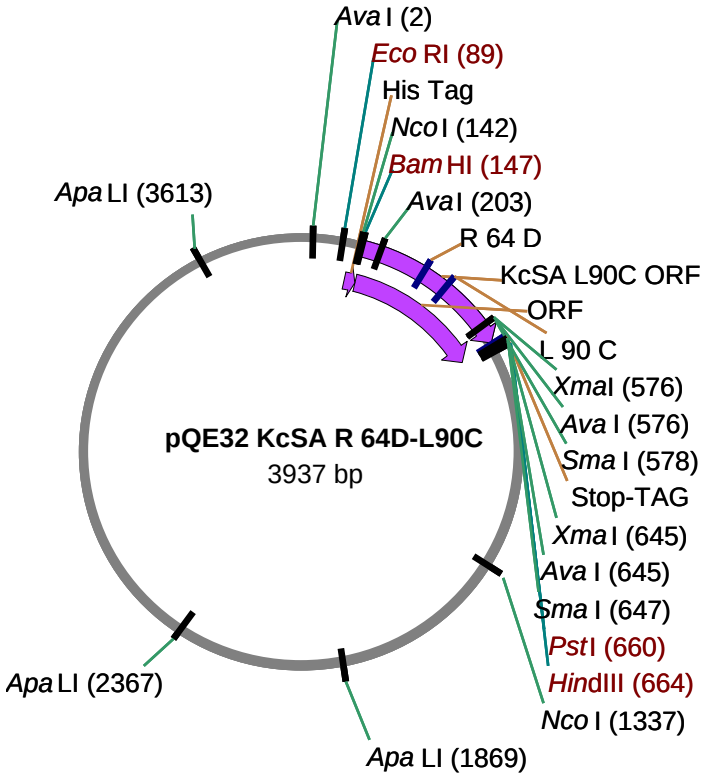
Ava I (2)
Eco RI (89)
His Tag
Nco I (142)
Bam HI (147)
Ava I (203)
R 64 D
KcSA L90C ORF
ORF
L 90 C
Xma I (576)
Ava I (576)
Sma I (578)
Stop-TAG
Xma I (645)
Ava I (645)
Sma I (647)
Pst I (660)
Hind III (664)
Nco I (1337)
Apa LI (1869)
Apa LI (2367)
Apa LI (3613)
pQE32 KcSA R 64D-L90C
3937 bp

8.3 Amino acid abbreviations and properties

Amino acid	3 letter code	1 letter code	polarity	charge
Alanine	Ala	A	nonpolar	neutral
Arginine	Arg	R	polar	positive
Asparagine	Asn	N	polar	neutral
Aspartic acid	Asp	D	polar	negative
Cysteine	Cys	C	nonpolar	neutral
Glutamic acid	Glu	E	polar	negative
Glutamine	Gln	Q	polar	neutral
Glycine	Gly	G	nonpolar	neutral
Histidine	His	H	polar	positive(10%) neutral(90%)
Isoleucine	Ile	I	nonpolar	neutral
Leucine	Leu	L	nonpolar	neutral
Lysine	Lys	K	polar	positive
Methionine	Met	M	nonpolar	neutral
Phenylalanine	Phe	F	nonpolar	neutral
Proline	Pro	P	nonpolar	neutral
Serine	Ser	S	polar	neutral
Threonine	Thr	T	polar	neutral
Tryptophan	Trp	W	nonpolar	neutral
Tyrosine	Tyr	Y	polar	neutral
Valine	Val	V	nonpolar	neutral

8.4 List of figures

8.5 List of tables

9 Acknowledgements

My sincere thanks to Prof. Dr. Olaf Pongs for choosing me as his student for a very good project and for supervision, advice and new ideas. His usual and regular phrase ‘Think or Sink’ made me atleast a good researcher in ion channel field. I am grateful to work under such a calm, cool and humorous but yet very professional person.

I would like to thank Dr. Sabine Lüthje for reviewing my thesis and act as a co-supervisor for my PhD studies.

I am especially grateful to Dr. Sönke Hornig, a perfectionist and a very good friend who has a lot of patience and always helped me throughout my work, suggested and supervised at each point. I thank him for reading my thesis and make useful comments.

I am grateful to Prof Dr. Jürgen Schwarz and Dr. Vitya Vardanyan for helping me out with some technical problems and for giving suggestions in electrophysiological experiments.

I am thankful to our collaborators Prof. Dr. Marc Baldus, Prof. Dr. Stefan Becker and Dr. Ulrich Zachariae for giving new ideas in the project and for publishing such a good papers.

I thank heartfully Iris Ohmert for helping me during my PhD with the molecular biology work, providing the clones whenever required and always keeping me in track without any mistakes. I am thankful to Elena Crenguta Dinu for being such a wonderful colleague and friend, always helping in professional and personal life.

I am especially thankful to all my colleagues in the lab Lijuan, Sasha, Gregor, Dragos, Uli, Malte, Wiebke, Martin, Dörte for providing suggestions, discussions and for creating a good environment in the lab. I would like to thank my ex colleagues and friends Quyen, Jacqueline, Alex, Jan, Christoph, Kathrin for making my life comfortable during my stay in Hamburg. I am thankful to my friends Sebastian, Satish and Eka for always providing continuous support and encouragement.

My heartful and sincere thanks goes to my friends Jai, Madan, Ravi, Raju, Satti, Manju, Bhavitha and Sujana for supporting and motivating me through out my life.

Last but the important people, I am grateful to my parents, my wife Sree and my cousin Kranthi who were and will always be with me encouraging and supporting.

I would like to dedicate my work to my dad who always believed that I would be a good student and will succeed in my life.